

Exploring the Potential of Polyelectrolyte- aptamer Films for Use in Optical and Electrochemical Sensing

Brian Malile

A thesis submitted to the Faculty of Graduate Studies
in partial fulfillment of the requirements
for the degree of
Master of Science

Graduate Program in Chemistry
York University
Toronto, Ontario

December 2015

© Brian Malile, 2015

Abstract

Polyelectrolyte-aptamer films have emerged as versatile and easy-to-fabricate materials for applications ranging from cargo delivery to sensing. The films comprising charged polymers and DNA aptamers exhibit changes in the permeability upon binding of the target. Herein we explore the target-controlled diffusion of ions in these films as the basis for generating sensing signals. First, we demonstrate a colorimetric sensing platform, where the polyelectrolyte-aptamer film is assembled on top of plasmonic nanoparticles. The colorimetric response arises from morphological changes of nanoparticles induced by an oxidizing etching agent, whose rate of diffusion is controlled by the polyelectrolyte-aptamer film. Second, we show the versatility of these films for electrochemical sensing by assembling polyelectrolyte-aptamer films on Indium Tin Oxide electrodes. Cyclic voltammetry was employed to monitor the diffusion-controlled electrochemical activity of a redox couple that generates the signal. We examine the concentration dependence and ionic interference effects of these two platforms, and investigate the film composition and aptamer requirements for achieving the sensing functionality. In summary, this project provides fundamental insight on a facile and low cost methodology in optical and electrochemical sensing that may be readily adapted to different analytes. Further development of these films and sensing platforms may allow portable field analysis by using consumer electronics. Our work presents new opportunities in aptamer-based sensing.

ACKNOWLEDGMENTS

I would like to thank Professor Jennifer Chen for her immense patience in showing me the world of research. She took me in as a fourth year undergraduate student without much experience in a research lab. She led by example and worked by my side to show me not only the fundamentals but the complex techniques. Her passion and dedication pushed me to ask the most from myself in research and in life. I entered her group as an undergraduate whose goal was to only graduate but I came out passionate and motivated for my future in chemistry. She has been a great teacher and mentor to me.

I would also like to thank my committee members Philip E. Johnson and William J. Pietro who provided useful tips on how to improve my research and also hard questions to give me incentive to understand more. I would like to express my gratitude for taking their time to read my thesis.

Finally, I would like to thank my family Laureta, Petrit and Tedi for their tremendous support throughout writing this project.

Table of Contents

| | |
|---|------|
| Abstract | ii |
| Acknowledgments | iii |
| Table of Contents | iv |
| List of Figures | vii |
| List of Schemes | xi |
| List of Equations | xii |
| List of Abbreviations | xiii |
| | |
| CHAPTER 1: Introduction | 1 |
| 1.1 Polyelectrolyte Films | 1 |
| 1.2 Aptamers | 5 |
| 1.3 Recent Progress on applications of polyelectrolyte-aptamer films | 7 |
| 1.4 Portable Sensors | 10 |
| 1.5 Scope Of Work | 12 |
| | |
| CHAPTER 2: Incorporation of polyelectrolyte-aptamer films with plasmonic nanoparticles for colorimetric sensing | 13 |
| 2.1 Introduction | 13 |
| 2.1.1 Localized Surface Plasmon Resonance (LSPR) | 13 |
| 2.1.2 Optical Methods Using Plasmonic Nanoparticles | 15 |
| 2.1.3 Previous Work | 16 |
| 2.1.1 Objective | 17 |
| 2.2 Experimental | 18 |
| 2.2.1 Materials | 18 |
| 2.2.2 Gold-Coated Silver Nanoprism Synthesis | 18 |
| 2.2.3 Transmission Electron Microscopy | 19 |
| 2.2.4 Preparation of APTMS Cover Slips and Deposition of AgNP on Glass | 19 |
| 2.2.5 Layer-by-Layer Polyelectrolyte Assembly on AgNP modified Cover Slips | 20 |

| | |
|---|----|
| 2.2.6 Target Binding and Film Development Procedures..... | 21 |
| 2.3 Results and Discussion..... | 23 |
| 2.3.1 Adapting Platform for the Detection of Quinine | 23 |
| 2.3.2 Ferricyanide as the Etchant..... | 25 |
| 2.3.3 Investigating Morphological Changes of the Nanoparticles..... | 28 |
| 2.3.4 Adjusting Experimental Times | 30 |
| 2.3.5 Concentration Dependence | 31 |
| 2.3.6 Ionic Interference | 33 |
| 2.3.6.1 Interference of Mercury (II)..... | 35 |
| 2.3.6.2 Interference of Sulfate..... | 37 |
| 2.3.7 Effect of Aptamer Folding on the Permeability of the Film..... | 40 |
| 2.4 Conclusions | 43 |
| | |
| CHAPTER 3: Modifying Electrodes with Polyelectrolyte-aptamer Film for Electrochemical Sensing | 44 |
| 3.1 Introduction | 44 |
| 3.1.1 Towards Miniature Electrochemical Systems | 44 |
| 3.1.2 Electrochemistry and Cyclic Voltammetry..... | 45 |
| 3.1.3 Objective | 46 |
| 3.2 Experimental | 47 |
| 3.2.1 Preparation and Modification of Electrodes | 47 |
| 3.2.2 Electrochemical Measurements | 47 |
| 3.2.3 Concentration Dependence and Ionic Interference..... | 48 |
| 3.2.4 Non-specific Binding..... | 48 |
| 3.2.5 Optimization | 49 |
| 3.2.6 Aptamer Folding | 49 |
| 3.3 Results and Discussion..... | 50 |
| 3.3.1 Effect of Base Bilayers | 51 |
| 3.3.2 Concentration Dependence | 51 |

| | |
|--|----|
| 3.3.3 Specificity of Detection | 53 |
| 3.3.4 Optimization | 55 |
| 3.3.5 Ionic Interference | 57 |
| 2.3.6 Effect of Aptamer Folding | 59 |
| 2.3.7 Peak Potentials and Diffusion Coefficients | 61 |
| 3.4 Conclusions | 63 |
| CHAPTER 4: Outlook and Future Work..... | 64 |
| 4.1 Summary | 64 |
| 4.2 Outlook and Future Work | 65 |
| References..... | 67 |

List of Figures

- Figure 1.1** Layer-by-layer assembly of polycations and polyanions on a charged surface to form multi layered thin films by successive deposition^[2] (adapted from [2]).1
- Figure 1.2.** Processes that take place during Systematic evolution of ligands by exponential enrichment for the generation of aptamers. Step 1: A library of DNA oligonucleotides is incubated with the potential target immobilized on a bead. Step 2: Non-binding strands are washed away. Step 3: Binding strands are eluted from the bead. Step 4: The Eluted strands are amplified through PCR.5
- Figure 1.3.** Fluorescence recovery after photobleaching (FRAP) for a single hollow polyelectrolyte-aptamer microcapsule (adapted from [3]). Area inside a microcapsule was bleached and the recovery of fluorescence intensity was monitored with time to characterize the permeability of film8
- Figure 1.4.** Principle of operation of typical biosensors. The receptor is conjugated with a transducer which generates a signal based on receptor-analyte interaction (adapted from [1])....10
- Figure 2.1.** Illustration of Localized surface Plasmon Resonance. Interaction with the electric field of light shifts the conduction electrons of the nanoparticle, giving rise to a dipole. The oscillation of this dipole results in intense colours (adapted from [4]).....13
- Figure 2.2.** Polyelectrolytes used in the layer-by-layer assembly, polystyrene sulfonate (PSS) and polyallylamine hydrochloride (PAH).....20
- Figure 2.3.** Representative experiment with the quinine aptamer (MN-19) incorporated in the film instead of the sulforhodamine B aptamer. (a) & (b) UV-Visible spectra of films during chemical development, over 75min. (c) Calculated areas of each peak are plotted against time. Binding of quinine to the aptamer leads to greater etching of the nanoparticles.....23
- Figure 2.4.** Spectra of nanoparticles during etching with ferricyanide. (a) Etching of bare nanoparticles immobilized on cover slip. (b) & (c) Etching of nanoparticles covered with 4 and 8 bilayers of polyelectrolyte. Ferricyanide is not able to etch the nanoparticles with the negative outer layer of PSS present.....25
- Figure 2.5.** Layers of polyelectrolyte-aptamer film on top of immobilized nanoparticles. The film consists of four base bilayers of PAH/PSS, eight bilayers of PAH/DNA, and a single PAH outer layer.....26
- Figure 2.6.** (a) Etching spectra of nanoparticles after the installation of a positively charged outer layer of PAH. (b) Etching spectra after the installation of a PAH layer on the original polyelectrolyte aptamer film. Capping the film with positive polyelectrolyte layer leads to increased interaction of the ferricyanide ions with the film...27
- Figure 2.7.** Transmission electron microscopy images before (a) and after (b) etching of the nanoparticles with ferricyanide. Particle size distribution before (c) and after (d) etching with

ferricyanide. Morphological changes on the nanoparticles are observed upon incubation with ferricyanide.29

Figure 2.8. New experimental setup with ferricyanide and spectral collection over the course of seven minutes. Spectral decay during etching of films incubated with water (a) and quinine (b). (c) Normalized peak intensity decay plotted against time. Extent of intensity decay of quinine bound film is twofold greater than that of the control.30

Figure 2.9. Concentration dependence experiments showing UV-visible spectra during etching in the first 10 min. Five films introduced to different concentrations of quinine ranging from 0-500 μ M. The control and 50 μ M (a) and (b), have similar LSPR decay while the higher concentrations(c)-(e) have greater peak decay...31

Figure 2.10. Effect of quinine on the permeability of polyelectrolyte-aptamer films. Effect of quinine is monitored as percent intensity decay of the LSPR of nanoparticles. Individual films were incubated in different concentrations of quinine. An average of six independent experiments, with SEM as error bars, shows a two fold increase in colorimetric response with increasing quinine concentration. (Inset) Visual colorimetric response.....32

Figure 2.11. Percent intensity decay of LSPR of the platform in the presence of various ions compared with that of water and quinine. Sulfate and Mercury (II) ions interfere with the platform but the rest of the ions show no significant effect. Six independent experiments performed with the exception of Hg^{2+} , Sn^{2+} , Pb^{2+} (N=3).Error bars are SEM..33

Figure 2.12. Effect of mercury on the nanoparticles monitored via LSPR. LSPR peak decreases in intensity and blue shifts upon incubation with mercury (II) ions.35

Figure 2.13. EDX spectra of nanoparticles incubated with and without mercury. (a) Spectra of as-synthesized gold-coated silver nanoparticles. (b) Spectra of gold coated silver nanoparticles after incubation with 1 mM mercury (II) chloride.....36

Figure 2.14. Etching of nanoparticles in the presence of water and sulfate. The presence of sulfate ion does not interfere with the etching process.37

Figure 2.15. Control experiment for the determination of sulfate interference. Platform was tested by replacing the MN19 aptamer by polyelectrolyte (PSS), Random DNA1, and Random DNA2. Results show that sulfate ions interfere in all three modifications of the film. Three independent experiments for each condition with SEM as error bars.....38

Figure 2.16. Normalized intensity decay of nanoparticles in a platform where MN19 was replaced with MN4 aptamer. The absence of a structural change in the MN4 aptamer results in almost identical intensity decay between control (water) and target bound film (quinine). The graph shows three independent experiments with SEM as error bars.42

Figure 3.1. (a) Typical cyclic voltammogram of an ITO electrode covered with polyelectrolyte-aptamer film. (b) Anodic peak currents of cyclic voltammograms of electrodes covered with different number of bilayers of PAH /PSS. Increasing number of bilayers means greater surface coverage and a lower peak current. Potential is scanned from -0.35V to +0.7V vs Ag/AgCl.

Concentration of ferricyanide is 60 μ M in 6mM KCl and the scan rate is 100mV/s. Triplicate experiments were performed with SEM as error bars50

Figure 3.2. Representative voltammograms of films on ITO electrode of 60 μ M potassium ferricyanide in 6 mM KCl at a scan rate of 100mV/s. (a) &(b) Voltammograms taken after incubation with the target (red line) line had higher anodic peak currents than voltammograms taken prior to incubation(black line). (c) The change in anodic peak current ($\Delta I_{p,a}$) obtained and plotted against increasing concentrations of quinine. The change in anodic peak current increases with increasing concentration of quinine with a saturation point at 200 μ M.(N=15 for 0 μ M an 350 μ M and N=4 for 50,150,250 and 500 μ M) Error bars are SEM.....51

Figure 3.3. $\Delta I_{p,a}$ of ecgonine compared with those of quinine and water. The response of ecgonine is similar to that of water suggesting no interaction with the aptamer. N=15 for water and quinine and N=3 for Ecgonine with SEM as error bars.....53

Figure 3.4. The effect of quinine on a random DNA oligonucleotide incorporated on the film. (Red) $\Delta I_{p,a}$ of quinine when MN19 aptamer is used. (Striped) $\Delta I_{p,a}$ of quinine when random DNA1 is used. Response of the platform when a random DNA is used is comparable to that of the control. Experiments with random DNA were done in triplicate. SEM was used for error bars.54

Figure 3.5. Response of platform in varying bilayers of PAH/PSS with the PAH/DNA-aptamer on top. Anodic peak currents of separate electrodes previously incubated in water followed by quinine. The anodic peak currents are comparable for the first three bilayers but a significant increase occurs in with four bilayers. Experiments were done in triplicate with SEM as error bars....55

Figure 3.6. Response of platform in varying bilayers of PAH/DNA. A slight increase in $\Delta I_{p,a}$ is observed when the number of PAH/DNA bilayers is increased from 4 to 12. Experiments were done in triplicate with SEM as error bars..56

Figure 3.7. Interference experiments characterized with cyclic voltammetry. (a) $\Delta I_{p,a}$ is obtained for the films exposed to a range of anions and cations with concentration of 1 mM. Sulfate is the only species which gives false positive results. The rest of the ions have responses comparable to the control (H₂O). Error bars are SEM57

Figure 3.8. Sulfate ions are precipitated with BaCl₂ prior to incubation with the platform. A smaller response is observed from the platform when sulfate ions are removed from solution. Experiments done in triplicate with SEM as error bars...58

Figure 3.9. $\Delta I_{p,a}$ of films comprising with the two versions of the same aptamer. MN19 aptamer folds into a three stem junction when binding to quinine and MN4 aptamer has a pre formed three stem junction and does not change when binding. An increase in $\Delta I_{p,a}$ is observed when the structure changing aptamer MN19 is used. Experiments done in triplicate for MN4 and SEM is used for error bars59

Figure 3.10. Scan rate dependence experiment of an ITO electrode modified with polyelectrolyte-aptamer film. (a) Cyclic voltammograms at increasing scan rates (10mV/s to 1000mV/s) of an electrode modified with polyelectrolyte-aptamer film. Inset shows linear dependence of peak currents with square root of scan rate. (b) Effect of scan rate on peak separation. Results show triplicate experiments with SEM as error bars.62

List of Schemes

- Scheme 2.1:** Integration of polyelectrolyte aptamer films with nanoparticles for optical sensing. The two stage sensor is first introduced to the target followed by a chemical development stage where the colorimetric signal is generated.....**16**
- Scheme 2.2:** (a) Cocaine binding aptamer MN19 folds upon binding to its target, quinine. (b) Quinine binding aptamer MN4 has a preformed secondary structure and does not change its conformation upon binding to quinine.....**41**
- Scheme 3.1** Film assembly on ITO electrode. Uneven film deposition leads to exposed areas of electrodes. Target binding causes swelling of the film and increases the diffusion of ferricyanide to the electrode surface. The increase in diffusion is observed as an increase in peak current in cyclic voltammograms**60**

List of Equations

| | |
|--|-----------|
| Equation 2.1 Extinction cross section for a nanoparticles with the diameter much smaller than the wavelength of light as described by the Mie-Rayleigh theory. The particle is assumed to be under uniform electric field | 14 |
| Equation 2.2 Dielectric function of a material such as silver. It is composed of a real part and an imaginary part | 14 |
| Equation 3.1 Randles-Sevick equation that shows the dependence of peak current on electrode area, concentration of analyte, diffusion coefficient, scan rate and number of electrons being transferred | 46 |
| Equation 3.2 Single-site binding equation for MN19-quinine interaction. | 52 |

List of Abbreviations

| | |
|--|---|
| PAH | Polyallylamine Hydrochloride |
| PSS | Polystyrenesulfonate |
| LbL | Layer-by-Layer |
| SAM | Self Assembled Monolayers |
| SELEX | Systematic Evolution of Ligands by Exponential Enrichment |
| FRAP | Fluorescence Recovery After Photobleaching |
| Au-g-C₃N₄ | Gold nanoparticle graphitic carbon nitride polymer |
| ECL | Electrochemilluminescence |
| hCG | Human Chorionic Gonadotropin |
| ITO | Indium Tin Oxide |
| LSPR | Localized Surface Plasmon Resonance |
| ϵ_{med} | Dielectric constant of the medium |
| ϵ_{real} | Real part of the dielectric function |
| ϵ_{im} | Imaginary part of the dielectric function |
| AgNP | Silver Nanoprisms |
| PVP | Polyvinyl Pyrrolidone |
| APTMS | Aminopropyltrimethoxy silane |
| TEM | Transmission Electron Microscopy |
| TMAI | Tetramethyl ammonium Iodide |
| EDX | Energy Dispersive X-ray |
| K_D | Dissociation Constant |
| keV | Kilo electronvolts |
| PBS | Phosphate Buffer Saline |
| I_{p,a} | Anodic Peak Current |
| I_{p,c} | Cathodic Peak Current |
| $\Delta I_{p,a}$ | Change in Anodic Peak Current |
| CV | Cyclic Voltammetry |
| SEM | Standard Error of the Mean |

CHAPTER 1: Introduction

1.1 Polyelectrolyte Films

Polyelectrolytes are polymers that have repeating units with charged groups which can dissociate in aqueous solution.^[6] Natural polyelectrolytes include proteins, DNA, and polysaccharides; in addition there are simpler synthetic polyelectrolytes as well, such as polyallyl amine hydrochloride (PAH) and polystyrene sulfonate (PSS). The degree of dissociation into polymer chains and counter ions determines the strength of the synthetic polyelectrolytes.^[6-7] A “strong” polyelectrolyte refers to a polycation or polyanion that is completely dissociated from its counter ions.^[2] A weak polyelectrolyte is one that partially dissociates into a charged chain and counter ions. The properties of polyelectrolytes are determined by the functional groups on the monomer, the type of counter ions, temperature, ionic strength and pH of the solution they are in.^[8] Exposed charges on polyelectrolyte chains allow for interaction with oppositely charged polyelectrolytes leading to formation of complexes in solution or multilayered thin films on a flat

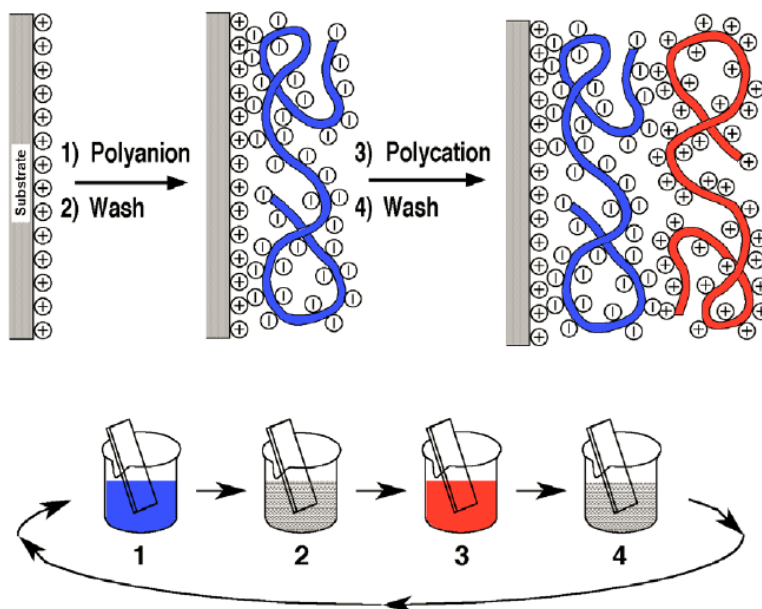


Figure 1.1 Layer-by-layer assembly of polycations and polyanions on a charged surface to form multi layered thin films by successive deposition^[2] (adapted from [2]).

substrates. Integration of other species into the films can provide control of permeability without the need of labels and chemical modification. These properties make these films highly desirable to be incorporated in sensing applications.

To form multilayered films, polyelectrolytes will adsorb on a surface with opposite charge to its functional groups. Once the surface is covered, the substrate can be rinsed and immersed into a solution with the oppositely charged polyelectrolyte. This procedure, illustrated in figure 1.1, is called layer-by-layer (LbL) assembly and was first developed by Decher et al.^[2, 6-7] The layer-by-layer method forms films comprised of oppositely charge polyelectrolytes. This method is used to deposit polyelectrolytes on flat surfaces to form films, and also on spherical templates which can be dissolved to form hollow microcapsules.^[9] Materials used for substrates can be glass, quartz, silicon, and gold. The forces drive the formation of the films consist of, electrostatic, hydrophobic, and hydrogen bonds. In addition to electrostatic interactions, gain in entropy due to release of counter ions, plays a major role in the assembly of the film.^[10]

The formation of films is a diffusion controlled process. Mass transport brings the chains close to the substrate surface for the adsorption to take place.^[11] Films consisting of PAH and PSS, have a 1:1 stoichiometry and the film growth is linear with each layer interpenetrating only the neighbouring ones.^[6] Properties of the films depend highly on the intrinsic properties of the individual polyelectrolytes (structure, charge density) and also, on the properties of the solution they are in (type of salt, and pH, ionic strength). Polyelectrolytes have like-charges in the chain and the chain conformation is stretched when floating in solution due to the electrostatic repulsion of these charges. Therefore, deposition conditions play a major role on the final film properties.^[12] High ionic strength in the polyelectrolyte solution leads to screening of the charges on the monomers, resulting in coiled secondary structures of the chains. When depositing, these coils

form thick and highly porous films. The absence of the salt in the polyelectrolyte solutions leads to straight chains due to the repulsion of the charges on the monomers. The straight chains dense films.^[13]

Multilayer growth starts with the adsorption of the first layer on the charged substrate. Most polyelectrolytes undergo linear growth during deposition.^[12] The morphology of the first few layers is drastically different from the rest of the film.^[11] The first few layers have uneven thickness and do not provide full coverage of the substrate surface. The factors that influence the uneven thickness are the surface morphology and the conformation of the polyelectrolyte chains during deposition.^[14] After the first few layers are deposited, the adsorption of polyelectrolyte does not depend on the charge of the substrate and uniform layers with more consistent thickness are formed.^[8] With enough layers deposited, further adsorption is hindered by the repulsion of the polyelectrolytes in solution and the polyelectrolytes with the same charge on the film.

Polyelectrolyte films are sensitive to humidity and water content. They can swell up to 40% of their thickness due to the hydration. The swelling depends on the interaction of the outer layer with water, with the outer layers of the films swelling to a greater extent than the inner layers.^[10] Addition of salt effects the swelling behaviour of polyelectrolytes. The swelling depends on the ionic strength, type of ion, and size. This effect can be attributed to the ranking of ions on the Hofmeister series. The Hofmeister series ranks ions on their ability to precipitate a protein.^[15] They are divided into chaotropes and kosmotropes. Chaotropes have weaker interactions with water than water itself and are called structure breakers. The kosmotropes have stronger interactions with the water molecules and are called structure makers.^[15] These factors determine how a particular polyelectrolyte film will behave depending on the conditions.

The layer-by-layer method has proven to be a more advantageous method than the self-assembled monolayers (SAM) and Langmuir-Blodgett films. Both SAMs and Langmuir-Blodgett films rely on weak molecular interactions and are not stable in physiological conditions. This instability leads to the “stripping” of adsorbates due to surrounding environment.^[16] Films assembled via LbL are stable in physiological conditions as well as in a wide range of pH, temperature and ionic strength.^[17] One important advantage of the LbL method is that a wide range of building blocks can be used to construct films. These building blocks include synthetic polyelectrolytes but also natural polymers such as DNA and proteins.^[17] The method is inexpensive and does not require complex instrumentation.^[14]

Multilayered thin films have shown versatility in a range of applications. They have been used in sensors^[18], nanofiltration^[19], coatings^[20], and surface modifications^[21]. Recent work makes use of target responsive thin films for potential sensing applications and construction of microcapsules which can be used for delivery.^{[22],[9]} Factors that determine the film thickness, permeability and ion transport include ionic strength and pH of the solution they are in prior to deposition.^[23] Polyelectrolytes explored for drug delivery, are assembled in capsules and only release their cargos in cells with a certain pH.^[24] Also, they are used for the development of sensors, in which changes in optical or electrochemical signals can be detected.^[17] These films are versatile tools that are easily constructed. They provide a flexible and dynamic medium for the immobilization of other species. Most commonly nucleic acids, enzymes and nanoparticles have been incorporated in these films.^[25] In this work we incorporate aptamers in polyelectrolyte films to control their permeability.

1.2 Aptamers

Aptamers are DNA oligonucleotides, obtained through Systematic Evolution of Ligands by Exponential Enrichment (SELEX), and bind with high affinity to their corresponding targets.^[26] SELEX is the method that selects aptamers. Aptamers have a specific three dimensional structure that bind to various targets ranging from small molecules to whole organisms.^[5] The binding of the aptamer to the target results form a combination of aromatic stacking, hydrogen bonds, van der Waals interactions, and structure compatibility.^[27] They have affinities and specificities compared to monoclonal antibodies. The selection of the aptamers starts with a library of DNA oligonucleotides, typically between 10^{13} and 10^{15} molecules, developed with combinatorial chemistry.^[28] The library of the oligonucleotides is incubated with a potential target. The strands that bind to the target are partitioned from the weakly bound or the unbound strands. Those that successfully bind are then amplified with polymerase chain reaction. Iterative cycles of binding,

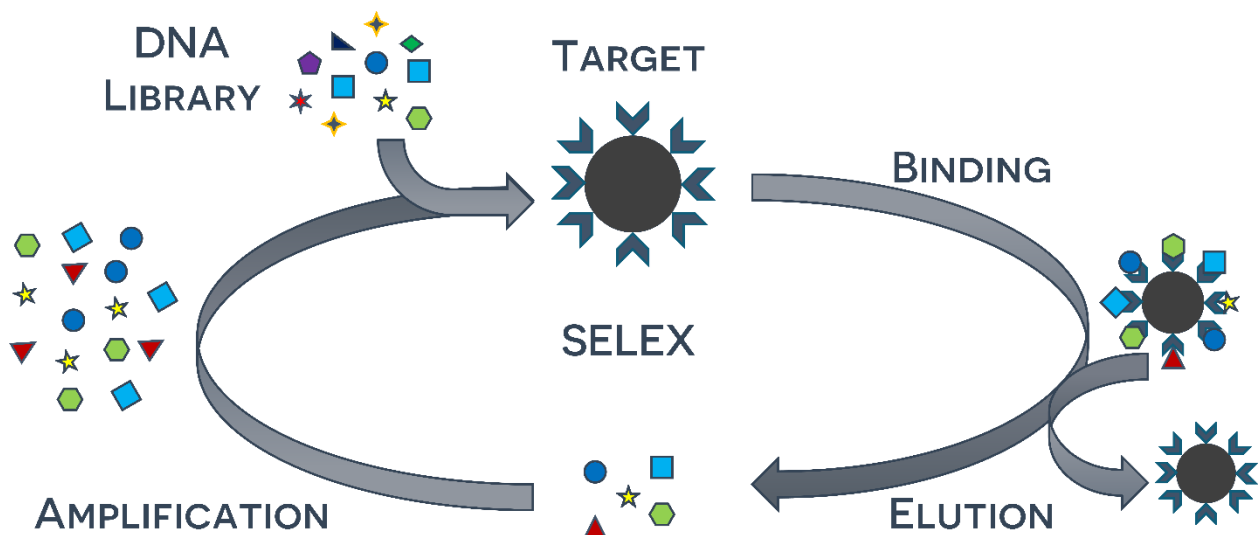


Figure 1.2. Processes that take place during Systematic evolution of ligands by exponential enrichment for the generation of aptamers. Step 1: A library of DNA oligonucleotides is incubated with the potential target immobilized on a bead. Step 2: Non-binding strands are washed away. Step 3: Binding strands are eluted from the bead. Step 4: The Eluted strands are amplified through PCR. ^[5]

partitioning and amplification are performed to select for the aptamer with the highest affinity and specificity to a target.^[5]

Aptamers have advantages over antibodies which make them more desirable for sensing applications and therapeutics. They are selected in vitro, which is a process much less expensive than the development of monoclonal and polyclonal antibodies.^[27] The selection process can be modified and unique features can be introduced to the aptamer. Furthermore, aptamers have the potential to be modified after the selection process. Functional groups for functionalization or reporter molecules can be attached for additional functionalities.^[5] They are stable at high temperatures and have a high shelf life. These properties have made aptamers a highly desirable new tool in various areas of research.

Aptamers have found their use in sensing and therapeutics. The most common example is the thrombin aptamer. Thrombin is an enzyme which has an important role in blood clotting.^[29] It plays an inhibitory role and prolongs the clotting. The interaction with thrombin makes this aptamer a potential agent for regulation of blood clots.^[26, 30] DNA aptamers have also shown inhibitory effects on the HIV1 enzymes. These enzymes play an important role on the lifecycle of the virus and are the common target for current HIV treatments.^[31] In addition to therapeutics aptamers have also been studied for the development of sensors.

The most common uses of aptamers in sensing have been in optical and electrochemical platforms. For optical sensing, fluorophores have been attached to conformationally relevant sites. The conformational change that the aptamer undergoes upon target binding changes the environment around the fluorophore enhancing or quenching the fluorescence.^[27] Aptamers have also been conjugated with gold nanoparticles. The binding of the aptamer to the target removes the aptamer from the surface of the nanoparticle leading to aggregation.^{[32] [32b]}

In addition to optical sensing applications, aptamers have been used for electrochemical sensing applications. They are more desirable for electrochemical sensors because the instrumentation is inexpensive and can be easily adapted for portable electronics. The most common approach for electrochemical sensing is the “signal on”/“signal off” method of detection. In these systems the aptamer is functionalized with a redox active species the proximity of which to the electrode depends on the secondary structure of the aptamer. In a study from Plaxco et al, the anti-cocaine aptamer is labeled with methylene blue and immobilized on the surface of an electrode. Without the target, the methylene blue is far from the electrode and the electron transfer is slow. After target binding, the secondary structure is more rigid and the methylene blue is closer to the electrode. The greater proximity of the redox active molecule to the electrode gives rise to faster electron transfer.^[33] The stability and versatility of aptamers makes them an invaluable tool for sensing applications and therapeutics.

1.3 Recent Progress on Applications of Polyelectrolyte-aptamer Films

Polyelectrolyte films respond to physicochemical stimuli such as pH, temperature, ionic strength. Incorporating these films with other materials can greatly expand their potential for applications. Aptamers are strands of DNA that bind with high affinity and specificity to an analyte. Due to the negative charge on the phosphate backbone of the DNA, they can be easily incorporated in these films. With the aptamer in the film, its permeability can be controlled through the binding of the analyte to the aptamer. Herein, a few methods are discussed to illustrate the control in permeability of polyelectrolyte-aptamer films on flat surfaces and spherical templates and their potential for sensing applications.

Microcapsules have been studied for their use in drug delivery.^[24] Microcapsules consisting of polyelectrolytes and sulforhodamine B aptamer were constructed on CaCO₃ spherical

cores. Once the deposition was completed the core was dissolved to form hollow microcapsules. Fluorescence Recovery After Photobleaching (FRAP) was used to study the diffusion of the dye through the walls of the microcapsules. Diffusion coefficients for the microcapsules incubated with the target were one order of magnitude higher compared with microcapsules used as control.^[3] Figure 1.3 illustrates how diffusion is monitored with FRAP.

Polyelectrolyte-aptamer multilayers can be constructed on flat surfaces to form films. Recent work shows that these films were deposited on top of a modified electrode with gold nanoparticle graphitic carbon nitride polymer (Au-g-C₃N₄).^[34] Au-g-C₃N₄ is a material which its

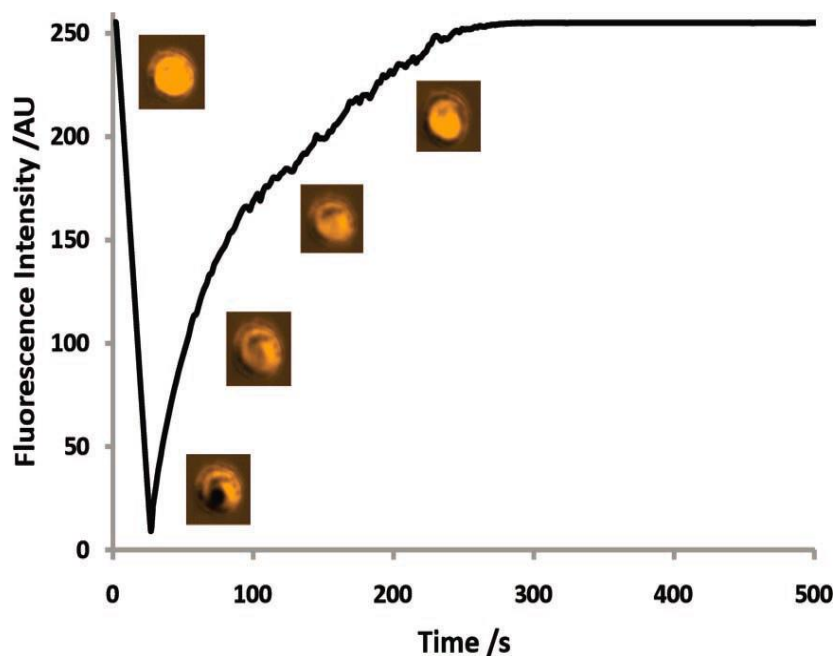


Figure 1.3. Fluorescence recovery after photobleaching (FRAP) for a single hollow polyelectrolyte-aptamer microcapsule (adapted from [3]). Area inside a microcapsule was bleached and the recovery of fluorescence intensity was monitored with time to characterize the permeability of film.^[3]

electrochemiluminescence (ECL) can be induced by persulfate ions. A glassy carbon electrode was modified with Au-g-C₃N₄ and a polyelectrolyte-aptamer films was deposited on top. The aptamer which binds to the model analyte Bisphenol A was used. When the target (Bisphenol A) is not present, there is no diffusion of the persulfate ions to the electrode and no ECL.^[22] With the

introduction of the target the permeability of the film increases and persulfate ions diffuse through to generate ECL.

Recent work from our group uses the permeability of polyelectrolyte-aptamer films to control the diffusion of an oxidizing agent that etches plasmonic nanoparticles to generate a colorimetric signal. The sulforhodamine B aptamer is used as a proof of concept. The polyelectrolyte-aptamer film was assembled on top of immobilized plasmonic nanoparticles. The platform was first incubated with the target then immersed in a solution of iodide/triiodide, which acts as an oxidizing agent.^[35] The oxidizing agent changes the size and shape of the nanoparticles therefore changing their plasmonic properties. Greater changes in morphology of the nanoparticles are observed when the aptamer is bound to its target compared with the control (no target) suggesting greater diffusion of the oxidizing agent. The oxidation of the nanoparticles is monitored via UV-Visible spectroscopy and the colour is discernible by naked eye.

The studies above illustrate the potential and universality of the polyelectrolyte-aptamer films. However more investigation is needed to understand the behaviour of these polyelectrolyte-aptamer films. An in-depth understanding of the polyelectrolyte-aptamer films allows for them to be utilized in various sensing applications. Their versatility lies with the facile incorporation of polyelectrolytes and aptamers.

1.4 Portable Sensors

There is a need to develop affordable technologies to improve healthcare, and environmental and food safety. Portable sensors should be simple, versatile and low cost, in addition to being highly selective and specific to the desired analyte. A sensor consists of a recognition element and a transducer.^[36] The recognition element interacts with the analyte,

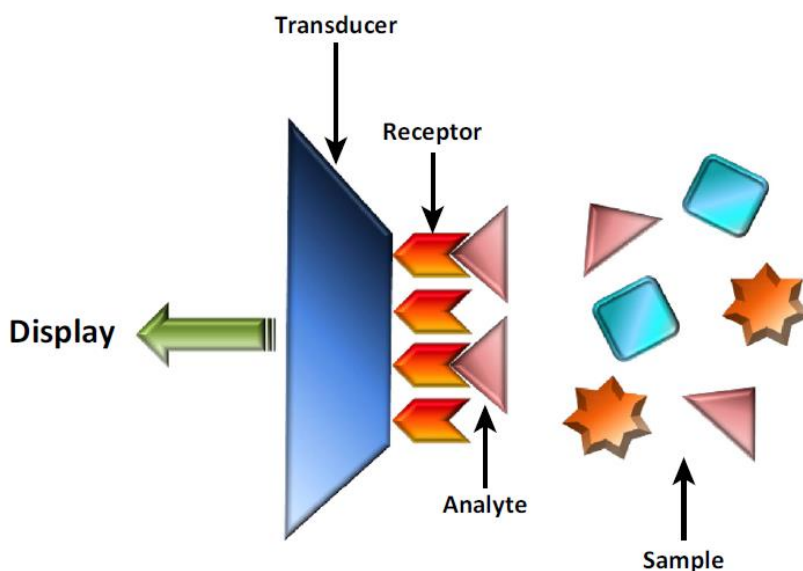


Figure 1.4. Principle of operation of typical biosensors. The receptor is conjugated with a transducer which generates a signal based on receptor-analyte interaction (adapted from [1]).^[1]

changing its properties (optical, structural, and electrical).^[36] A transducer converts these changes into a signal. Common recognition elements are antibodies, enzymes and aptamers while the transducing methods can be optical, piezoelectric and electrochemical.^[37]

Antibody sensors or immunosensors make use of an antibody-antigen interaction to generate a signal. Antibodies can be immobilized on surfaces of electrodes or plasmonic nanoparticles. Enzymes have also been used for biosensing.^[38] The products of the reaction catalyzed by the enzyme can be analyzed by a transducer.^[39] They have been used to detect molecules which inhibit or enhance their function. DNA oligonucleotides (Aptamers) are also

finding their way in sensing platforms. They work in the same fashion as antibodies however are more stable and can be easily synthesized without the need of animals or cells.^[40] The above recognition elements are the most common ones used in biosensing research and applications.

The most common transducers are piezoelectric, optical, and electrochemical. Piezoelectric transducers consist of crystals with mass sensitive oscillations and are connected to electrodes. Under unique electric fields the crystals are under resonant frequency. Binding events can influence the resonant frequency, the change of which can be converted into a signal.^[41] For optical sensors, the binding event can cause changes in absorbance, scattering and luminescence. All of the above responses can be analyzed and transduced into a signal.^[37] Electrochemical sensors which measure the changes in potential during an interaction are called potentiometric sensors.^[42] Sensors which measure impedance, monitor the resistance and capacitance of targets as a function of an excitation signal.^[43] These sensors work by monitoring the change in impedance arising from the binding of analytes to the receptors. Amperometric systems measure the changes in current due to the oxidation and reduction of an electroactive species.^[44] These sensors are used for analytes of redox active species.

A common point-of-care bio-diagnostic tool using nanomaterials is the home pregnancy test. It is a sandwich-type immunoassay where the antibodies, which bind to the human Chorionic Gonadotropin (hCG) hormone, are linked with plasmonic gold nanoparticles.^[45] This method uses lateral flow where the sample is introduced to the platform by capillary forces. Antibodies linked with gold nanoparticles, bind to the analyte (hCG) and flow to immobilized antibodies which also bind to hCG hormone. This interaction forms a sandwich and the colour is observed from the nanoparticles.^[46] Another example of a point of care device is the electrochemical analyzer iSTAT.^[47] It is completely automated and can give information on electrolytes, hematology and

cardiac markers from blood samples. The sample is introduced in cartridges and analytes are quantified through amperometric and potentiometric measurements.^[48]

Rapid, low-cost, and user-friendly sensing applications can provide improvements in diagnosis and also patient monitoring. Portable biosensors will improve personalized health monitoring. User-friendly platforms can help diagnose diseases at earlier stages and improve the overall treatment. Also, they can provide a tool for patients to self-manage chronic diseases. With the increase in research on portable biosensors, the prevention, diagnosis and treatment of diseases can be made much easier.

1.5 Scope of Study

The objective of this study is to comprehensively explore the polyelectrolyte-aptamer films. The focus of the investigation is to explore and understand the change in permeability of the polyelectrolyte-aptamer film upon interaction with the target. Furthermore, we aim to show the versatility of these films not only with different recognition elements (aptamers) but also with different transducers (optical, electrochemical). Also, we provide insight on the type of aptamers that can be used, determine interference species and optimize the films for maximum response. A previously developed proof-of-concept method for the detection of sulforhodamine B^[35] is adapted for the detection of cocaine/quinine. The film is incorporated with plasmonic nanoparticles for optical detection; in addition it will be investigated by assembling it on an ITO electrode for electrochemical sensing. Using these two methods we show the universality of the polyelectrolyte-aptamer films. Further development and characterization of this sensing platform will shed light on new approaches in aptamer-based sensing. With increasing libraries of aptamers, they can simply be incorporated in the same platform through electrostatics and be explored for the detection analytes such as ATP, Thrombin and other species.

CHAPTER 2: Incorporation of polyelectrolyte-aptamer films with plasmonic nanoparticles for colorimetric sensing

2.1 Introduction

Colorimetric sensors are desirable methods of detection because they generate rapid responses which can be analyzed visually. They are user friendly and provide rapid identification of problems with the drawback of providing qualitative rather than quantitative results. Plasmonic nanoparticles are widely used for colorimetric sensing.^{[49],[50]} They provide colorimetric signals through absorption and scattering of light. The colorimetric response originates from a unique property of noble metal nanoparticles, Localized Surface Plasmon Resonance (LSPR).

2.1.1 Localized Surface Plasmon Resonance (LSPR)

In a bulk material, a plasmon is the collective oscillation of the free electrons at the plasma frequency. Surface plasmon resonance (SPR) refers to surface propagating plasmons which are optically excited but confined to the surface of a metal.^[51] Localized surface plasmon resonance occurs in nanoparticles with dimensions much smaller than the wavelength of light. Due to the small size of metal nanoparticles, their surface to volume ratio is high and the majority of the

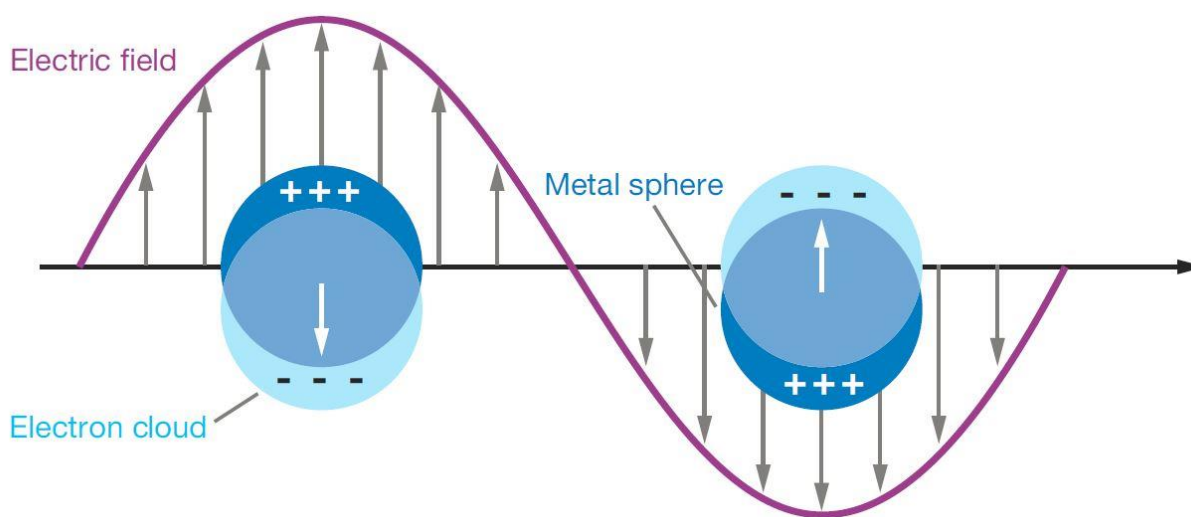


Figure 2.1. Illustration of Localized surface Plasmon Resonance. Interaction with the electric field of light shifts the conduction electrons of the nanoparticle, giving rise to a dipole. The oscillation of this dipole results in intense colours (adapted from [4]).^[4]

conduction electrons are on the surface of the nanoparticles. Light of certain frequency can cause electrons to collectively oscillate, resulting in strong absorption and scattering phenomena which produce intense colours.^[52] This phenomenon is known as localized surface plasmon resonance (LSPR) and is depicted in figure 2.1. The effect of the light on the nanoparticles is described by the Mie-Rayleigh theory (Equation 2.1), which calculates the extinction cross section of a nanoparticle.^[4]

$$C_{ext} = \frac{18\pi\epsilon_{med}^{1.5}V}{\omega} \frac{\epsilon_{im}(\omega)}{[\epsilon_{real}(\omega)+2\epsilon_{med}]^2 + \epsilon_{im}(\omega)} \quad (2.1)$$

The extinction cross-section is a summation of scattering and absorbing events and depends on particle volume (V), wavelength of incident light (ω), dielectric constant of the medium (ϵ_{med}) and the dielectric function of the metal (ϵ_{real} and ϵ_{im}).^[52] The Mie-Rayleigh theory describes the behaviour of the plasmons under the quasistatic approximation, which assumes that the particle experiences uniform electric field due to its small size. From the equation above, the extinction cross-section is maximized when the real part (ϵ_{real}) of the dielectric function from the metal is approximately $-2\epsilon_{med}$.^[53]

Due to the unique dielectric functions of silver and gold, their LSPR occurs in the visible regions, while for other metals it occurs in the ultraviolet. The real part of the dielectric function (equation 2.2) governs the peak position and the imaginary part governs the damping of the oscillations and the peak broadening.

$$\epsilon_m(\omega) = \epsilon_1(\omega) + i\epsilon_2(\omega) \quad (2.2)$$

The imaginary part of the dielectric function for silver is much smaller than that of gold, making the LSPR peaks from silver nanoparticles sharp and intense.^[54] The LSPR produces an extinction peak in the UV-Visible spectrum.

The size and shape of the nanoparticles as well as the surrounding medium have a great influence on the LSPR.^[53] LSPR is highly dependent on the refractive index of the medium. A high refractive index of the medium leads to a redshift of LSPR wavelength due to delayed oscillations.^[4, 55] The delayed oscillations occur from the temporary transfer of electrons to the surrounding medium. This transfer causes the electrons to lose energy and produce inelastic scattering, which causes peak broadening. Also high aspect ratio nanoparticles have more sensitive LSPR peaks than low aspect ratio nanoparticles (spheres).^[56]

The intense colours of noble metal nanoparticles are highly dependent on the size, shape, material, and surrounding medium. A small change in these factors will result in a change in their LSPR peak position and intensity.^{[4],[53]} While gold nanoparticles are widely explored, there are fewer reports of using silver nanoparticles for sensing. Due to their dielectric function, silver nanoprisms (Ag NP) can potentially provide higher sensitivity than gold nanoparticles and they also have higher extinction coefficients.^{[57],[58]} In the triangular prism shape, the plasmon bands can be tuned throughout the entire visible-IR wavelength range by controlling the particle's size and shape. Because the optical properties are very sensitive to changes in the morphology of silver nanoparticles, they provide new promises for sensing applications.

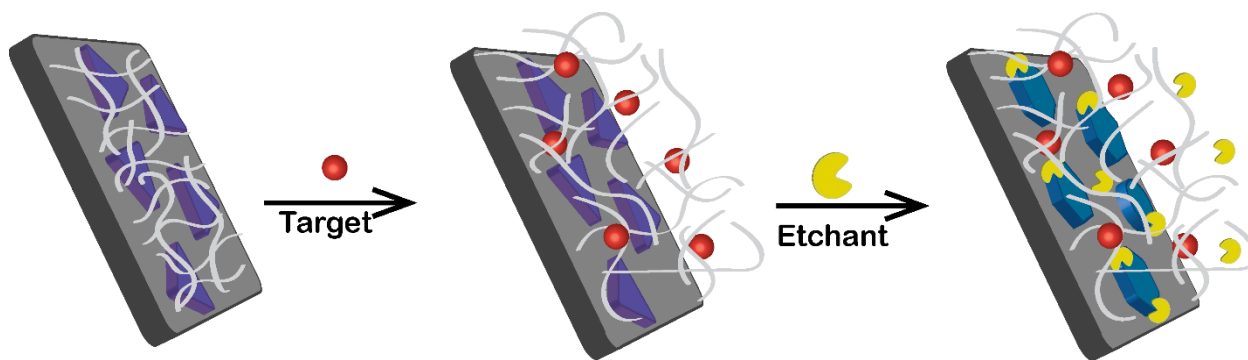
2.1.2 Optical Methods Using Plasmonic Nanoparticles

There have been varieties of methods developed that use a change in the size, shape and environment of the nanoparticles to generate a colorimetric signal. Aggregation-based sensors generate a colorimetric signal because the interparticle distance can influence the LSPR. Particle aggregation causes plasmon hybridization and an increase in the refractive index of surrounding medium leading to a change in LSPR properties.^[32b] One of the main limitations of these methods is that they are restricted to solution-based testing. This restriction hinders the portability of the

device for its performance in the field. Other studies show the generation of the colorimetric signal, for the detection of mercury or copper, by inducing a change in the shape of the nanoparticles.^{[59],[60]} They require the analyte to chemically react with the nanoparticles and therefore can only be applied to specific analytes. This work aims to introduce easily adaptable and universal components that can be incorporated with nanoparticles. Improvements on portability and storage can be made by employing dipstick type sensors for detection of analytes in complex media. Sensing in complex media is highly desirable because it provides rapid results and requires less expertise for sample preparation.

2.1.3 Previous Work

Previously we developed a platform that uses gold-coated silver nanoparticles for colour generation and polyelectrolyte-aptamer films for target interaction. The demonstration used sulforhodamine B, a fluorescent dye, as a proof of concept. Scheme 2.1 shows the basic principle of operation of this platform. Gold-coated AgNP were immobilized on substrate and a polyelectrolyte-aptamer film was deposited on top. This platform works in two stages. In the first stage, we introduce the sensor to the target, the binding of which causes swelling of the polyelectrolyte-DNA overlayer. In the second stage, we expose the sensor to an etchant, which will, diffuse through the film, and change the morphology of the nanoparticles thus generating a



Scheme 2.1. Integration of polyelectrolyte aptamer films with nanoparticles for optical sensing. The two stage sensor is first introduced to the target followed by a chemical development stage where the colorimetric signal is generated.

colorimetric response. Because the biological gate controls the diffusion of the etching agent, a control film (no target) would exhibit a different colorimetric signal when compared with a film with the target bound upon chemical development. With further investigation, the polyelectrolyte-aptamer film has the potential to be a universal component for sensing platforms.

2.1.4 Objective

The first goal is to replace the sulforhodamine B aptamer with the cocaine/quinine binding aptamer while maintaining functionality of the platform. Quinine does not absorb in the visible region and therefore does not interfere with the optical characterization of the platform. Second, we aim to replace the oxidizing agent, triiodide, with something more versatile and stable such as ferricyanide. Ferricyanide can act as an oxidizing agent for the etching of nanoparticles; additionally it can serve as a redox active probe for subsequent electrochemical measurements. Third, concentration dependence and interference experiments provide insight on the detection range and the integrity of the platform in complex media. Lastly, the effect of aptamer folding is investigated by comparing two versions of the same aptamer which differ in structure changing ability upon target binding. This chapter investigates in detail how the control of the permeability of the polyelectrolyte-aptamer film can be used for colorimetric sensing.

2.2 Experimental

2.2.1 Materials

Silver nitrate (AgNO_3), Sodium borohydride (NaBH_4), Sodium citrate dihydrate, L-Ascorbic acid, Hydrogen peroxide 30 wt%, Polyvinylpyrrolidone (PVP), MW 96000, Diethylamine, Potassium iodide KI, Hydrogen tetrachloroaurate (III) trihydrate ($\text{HAuCl}_4 \cdot 3\text{H}_2\text{O}$), aminopropyltrimethoxy silane (APTMS), Polyallylamine hydrochloride (PAH) MW 56000, Polystyrenesulfonate (PSS) MW 100000, were purchased from Sigma Aldrich. MN-19, sequence 5' - *GAC AAG GAA AAT CCT TCA ACG AAG TGG GTC*- 3', MN4, sequence 5'- *GGC GAC AAG GAA AAT CCT TCA ACG AAG TGG GTC GCC*-3', Random DNA1 sequence 5'- *CTG TGC GTG TGA CAG CGG CTG A* -3' and Random DNA2 5'- *CTT TCG CGC ATG ATT GAA AAC AAT CAT GCG TAC GAG TTG AGA* - 3' were purchased from IDTDNA. Anhydrous Ethanol, 2-propanol were purchased from Commercial Alcohols. Quinine HCl was obtained from Sigma Aldrich.

2.2.2 Gold-Coated Silver Nanoprism Synthesis

In a typical synthesis of silver nanoprisms^[61], 50 mL of 0.1 mM silver nitrate was mixed with 3 mL of 30 mM of sodium citrate dihydrate under vigorous stirring. 120 μL of H_2O_2 30 wt% was added. Immediately after the addition of peroxide, fresh 200 or 180 μL of 0.1 M NaBH_4 was also added. The reaction was then allowed to proceed for 30 min. The contents were then centrifuged and washed with 1 mL of 3 mM sodium citrate once. The particles above were then dispersed in 9 mL of H_2O . To proceed with the vertical growth, 1 mL PVP 0.0175 M and 37.5 μL of 0.5 M ascorbic acid, which was made fresh, were added to the redispersed particles. Then, 0.6 mL of 0.6 mM of AgNO_3 was added via syringe pump at 6 mL/h. To the above solution 300 μL of 30 mM citrate was added followed by the addition of a growth solution of 0.75 mM AgNO_3 and 1.13 mM citrate via syringe pump at 6 mL/h. The UV-Vis spectra was taken to monitor the size of

the particles. The amount of growth solution added varies with each batch depending on the desired peak position. On average, 2.0 mL of the growth solution was added to keep the peak position at around 540-560 nm. The reaction was allowed to proceed for 1 hour.

To proceed with the gold coating, 1 mL of PVP 5 wt%, 200 μ L of 0.5 M ascorbic acid, and 150 μ L of diethyl amine were added to the AgNP solution. A separate gold solution was prepared by mixing 1.37 mL of H₂O, 100 μ L PVP 5%, 20 μ L 0.2 M KI, and 5 μ L of 0.25 M of H₂AuCl₄·3H₂O which was added through a syringe pump at a rate of 1 mL/h. Upon completion, the reaction was allowed to proceed for 0.5-1 h.^[62] The gold coated AgNP were cleaned via centrifugation and were redispersed in 1 mL of H₂O for storage.

2.2.3 Transmission Electron Microscopy (TEM)

To investigate the morphological changes of the nanoparticles, a representative sample solution was concentrated by spinning down the newly synthesized nanoparticles. Another batch of nanoparticles was introduced to 1 mM of potassium ferricyanide for 10 minutes and concentrated via centrifugation. The two concentrated batches were deposited by evaporating on copper grids for TEM imaging. The images were analyzed with ImageJ software and the histograms were constructed by counting the frequency of the sizes of nanoparticles. The size of the nanoprisms was determined to be the distance between one of the vertices to the opposing side.

2.2.4 Preparation of APTMS Cover Slips and Deposition of Ag NP on Glass

The cover slips (VWR micro cover glass 25 mm x 25 mm) were placed in the plasma cleaner (Harrick's PDC-32G) for 15-20 minutes. After the cleaning, the cover slips were placed in 1% APTMS solution. The beaker was covered and the cover slips were left for 2 hours for silanization. Then, the cover slips, were quickly rinsed and dried. The substrates were placed on a hot plate for annealing under nitrogen atmosphere overnight. These substrates were then cut up in six sections

to be used as substrates for nanoparticle deposition. For the deposition of the silver nanoprisms onto the glass substrate, the particles were diluted three times from the storing concentration. The glass piece was put on particle solution for 30-60 seconds, removed, rinsed with isopropanol and dried before the next immersion. This procedure was repeated two or three times for the desired intensity on the substrate.

2.2.5 Layer-by-Layer Polyelectrolyte Assembly on AgNP Modified Cover Slips

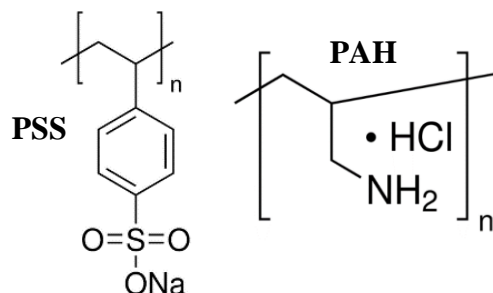


Figure 2.2. Polyelectrolytes used in the layer-by-layer assembly, polystyrene sulfonate (PSS) and polyallylamine hydrochloride (PAH).

Solutions of PAH and PSS, shown in figure 2.2, were made by dissolving 2 mg/mL of polyelectrolyte in 0.2 M NaCl. DNA aptamer was dissolved in a 1x Phosphate Buffer Saline (PBS) solution with 0.2 M NaCl at a concentration of 4.5 μ M. Layer-by-layer assembly was carried out using a robotic dipper (Microm DS 50). In a single layer deposition, the films were placed for 10 minutes in the polyelectrolyte solution followed by two rinsing steps. The deposition procedure was adapted from work done by De Rosa et al.^{[3, 63] [63]} After the rinsing steps for the positive electrolyte the same steps were repeated for the negative polyelectrolyte. Depending on the architecture of the film, different polyelectrolyte solutions were used. For example, the film (PAH/PSS)₄(PAH/DNA)₈ initially has four bilayers of PAH/PSS programmed. Once the four base bilayers of PAH/PSS were built the PSS solution was replaced with the DNA-aptamer solution

containing 4.5 μM cocaine binding aptamer. The deposition continued until eight bilayers were built. The films were kept hydrated at all times.

2.2.6 Target Binding and Film Development Procedures

After the Layer by layer deposition the films were introduced to the target, quinine. One film was kept as a control (in water) the other was put in 50 μM quinine for 1 hour. After, the films were rinsed and prepared for development. The first spectra of the films was taken in water. The water was replaced by I^-/I_3^- solution or ferricyanide solution.

Stock solutions of 0.1 M TMAI and 1.1 mM I_2 were prepared. The etchant was made fresh with the final concentration of 1 mM TMAI and 0.011 mM I_2 . For experiments with ferricyanide as the etchant, a concentration of 60 μM was used. The glass substrates were placed in a plastic cuvette and the initial spectrum was taken in water. After, the water was removed and 600 μl of ferricyanide solution was placed in the cuvette together with the film for etching. The spectra were taken every five minutes up to 75 minutes using a Cary UV-Vis spectrophotometer. The spectral collection was later decreased to three spectra taking 10 min in total.

The concentration dependence and ionic interference experiments were performed based on the same principle but with more films. Six films were used for concentration dependence starting with the control, 50 μM , 100 μM , 250 μM , 350 μM , 500 μM Quinine HCl. The ions tested were 500 μM of each of the following salts: MgCl_2 , MgSO_4 , NaHPO_4 , NH_4Cl , LiCl , PbCl_2 , HgCl_2 , SnCl_2 , NaSO_4 and KCl . To determine the effect of sulfate ions on the films, three types of platforms were constructed. One platform consisted of eight bilayers of PAH/PSS. Random DNA strands (RandomDNA1 and Random DNA2) were incorporated in the other two platforms. They were introduced to 500 μM of Na_2SO_4 for 30 min and spectral collection was done during the etching.

To determine the interaction of mercury with the nanoparticles, as-synthesised gold-coated silver nanoprisms were diluted and incubated with mercury. UV-Visible spectra was taken before and after incubation. Both batches of particles, with and without mercury were concentrated, washed two times and resuspended in ethanol. They were then deposited on ITO coated glass through evaporative deposition. Energy Dispersive X-ray measurements were performed to determine whether mercury was deposited on the nanoparticles. The accelerating voltage was 20 kV.

To test whether a structural change in the aptamer affects the response of the platform, the MN19 aptamer was replaced with the MN4 aptamer during the film deposition procedure. The target binding and film development procedures were done in the same way as the previous experiments.

2.3 Results and Discussion

2.3.1 Adapting Platform for the Detection of Quinine

We replaced the original sulphorhodamine B aptamer with the MN-19 aptamer, which binds to cocaine and quinine, and carried out the etching experiments. Two identical films with four bilayers of (PAH/PSS) and eight bilayers of (PAH/MN-19) were built. One film was introduced to the target (quinine) and the other was kept as a control (in water) for 1 hour. Figures 2.3a and 2.3b show the spectra collection of both the control and quinine bound film during chemical development, with iodide/triiodide, over the course of 75 minutes. Figure 2.3c shows the normalized area under each curve versus time. From the spectra in figure 2.3a and 2.3b, it is clear that the extinction peaks of film incubated with quinine have a faster decay rate than the film incubated in water. The greatest peak decay occurs in the first few minutes and can be observed in the first two peaks under each condition. For the control experiment, the peak intensity decays from 0.33 to 0.25, while that of the quinine experiment decays from 0.32 to 0.2. These results suggest that incubating the platform with quinine increases the permeability of the film. The greatest difference in decay occurs in the first 10 minutes of the etching. One explanation could be that during this time, the movement of the triiodide molecules through the film to the nanoparticles

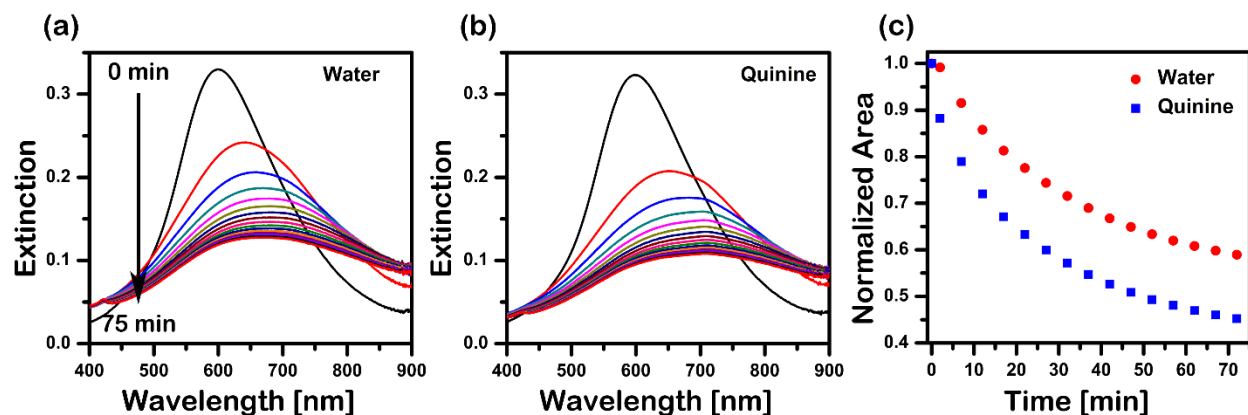


Figure 2.3. Representative experiment with the quinine aptamer (MN-19) incorporated in the film instead of the sulforhodamine B aptamer. (a) & (b) UV-Visible spectra of films during chemical development, over 75min. (c) Calculated areas of each peak are plotted against time. Binding of quinine to the aptamer leads to greater etching of the nanoparticles.

is governed by genuine diffusion. Whereas after some time, the film begins to saturate with etchant molecules and other factors such as surface chemical reactions start to have an effect.

This experiment shows that by simply replacing the aptamer during the film deposition, the platform can be adapted for the sensing of other targets and a similar colorimetric response can be obtained by the end of the chemical development. While initial studies looked promising, we observed variations upon the development of the film by the I/I_3^- etchant. The triiodide species is effective at etching gold and silver however, it is formed by the equilibrium between iodine and iodide ions in a solution. We observed the variation of triiodide concentrations between samples and over time. Hence, a new etchant was sought.

2.3.2 Ferricyanide as the Etchant

Based on the limitations stated above, we started to use $K_3Fe(CN)_6$ as the new oxidizing agent. Ferricyanide ions have been used for the mild etching of gold for patterning and for the shaping of nanoparticles.^{[64], [65]} The ferricyanide solution can be prepared from the salt and is more stable in comparison with triiodide. Moreover, the ferricyanide molecule has a (3-) charge and is much bulkier than the iodide/triiodide couple. We hypothesized that the molecule would have slow diffusion and enhance the difference in colorimetric response between the control film and the target bound film. In the first few experiments using ferricyanide, the particles did not etch when embedded under the polyelectrolyte film. Figure 2.4a shows the etching spectra of bare gold-coated silver nanoprisms immobilized on a glass surface vs those covered with four (Figure 4b) or eight (Figure 2.4c) bilayers of PAH/PSS film. Etching is evident from the decrease in peak intensity for the bare nanoparticles; however, the minimal decrease in peak intensity (Figure 2.4b

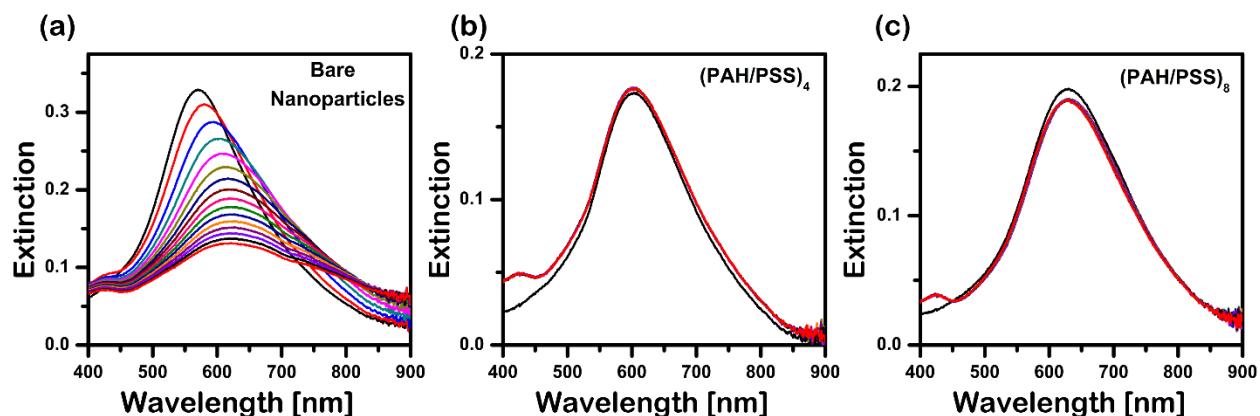


Figure 2.4. Spectra of nanoparticles during etching with ferricyanide. (a) Etching of bare nanoparticles immobilized on cover slip. (b) & (c) Etching of nanoparticles covered with 4 and 8 bilayers of polyelectrolyte. Ferricyanide is not able to etch the nanoparticles with the negative outer layer of PSS present.

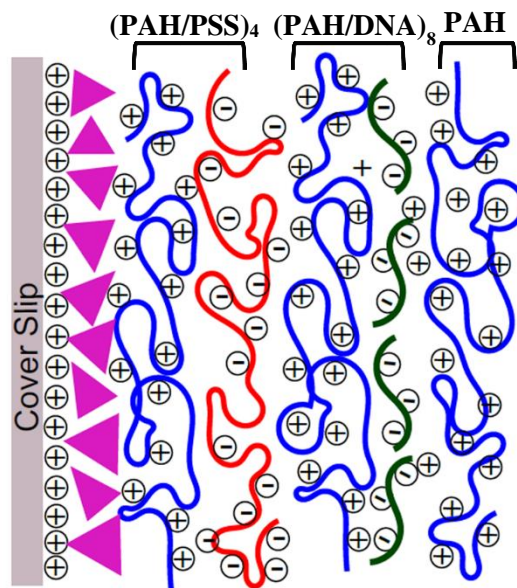


Figure 2.5. Layers of polyelectrolyte-aptamer film on top of immobilized nanoparticles. The film consists of four base bilayers of PAH/PSS, eight bilayers of PAH/DNA, and a single PAH outer layer.

and c) shows that etching does not take place on the nanoparticles covered with polyelectrolyte film. The etchant could not diffuse through the film.

Our hypothesis was that the outermost PSS layer, which is negatively charged, repels the ferricyanide ions and hinders their diffusion. To enhance the interaction of polyelectrolyte film with the etchant ions, a single outermost layer of positive polyelectrolyte (PAH) was installed. We hypothesize that a positive charge on the surface of the film would increase the interaction between the film and ferricyanide ions leading to greater diffusion. We then installed an outermost PAH layer as shown in Figure 2.5. Figure 2.6a displays the etching spectra after the installation of the PAH layer on a film with four bilayers of PAH/PSS. Results confirm our hypothesis that, with the installation of the outermost PAH layer, the interaction between ferricyanide and the film has increased leading to greater etching of the nanoparticles. Replacing iodide/triiodide with ferricyanide increased the reproducibility of experiments.

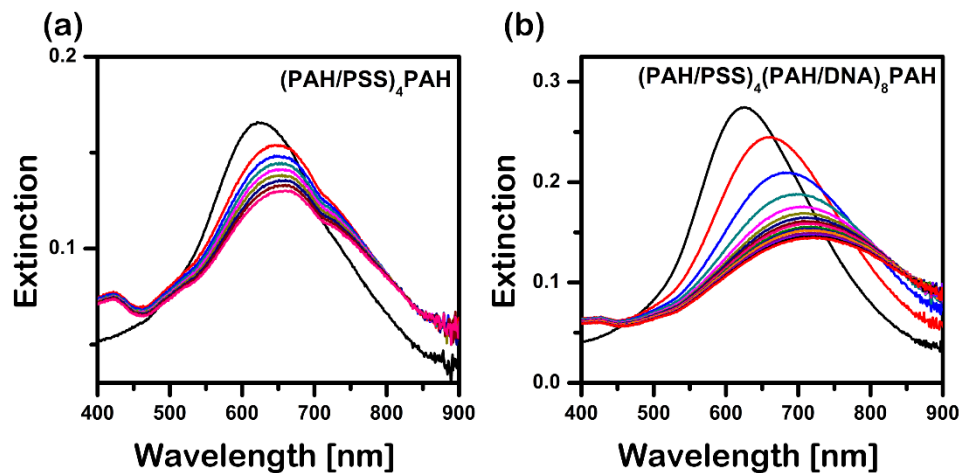
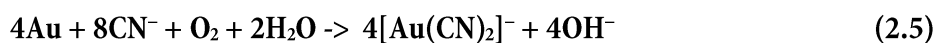
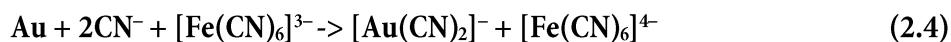


Figure 2.6. (a) Etching spectra of nanoparticles after the installation of a positively charged outer layer of PAH. (b) Etching spectra after the installation of a PAH layer on the original polyelectrolyte aptamer film. Capping the film with positive polyelectrolyte layer leads to increased interaction of the ferricyanide ions with the film.

2.3.3 Investigating Morphological Changes of the Nanoparticles

The reactions below show possible pathways in which the gold is etched with ferricyanide. The coordination of cyano group to the gold reduces its oxidation potential for the iron complex



to remove one electron. Even though the dissociation of a cyano ligand from the iron complex has a low K_D (reaction 2.3), reactions 2.4 and 2.5 are thermodynamically favourable and could aid in the formation of free cyano species. The same reactions are proposed for the oxidation of silver with ferricyanide as well.^[66]

The etching of nanoparticles in solution leads to a blue shift of their LSPR peak which corresponds to smaller particles.^{[56], [51]} The etching in our setup shows a decrease in peak intensity and a redshift of the extinction peak. This redshift could be due to the position of the nanoparticles in the setup. They are sandwiched between a glass substrate and a polyelectrolyte aptamer film. The etching therefore does not proceed in the same fashion as when they are floating freely in solution. During the etching process, the products of the reactions (dicyano aurate) could remain on the surface of the nanoparticles. The deposition of the products on the surface of the nanoparticles changes the refractive index of the surrounding medium and causes a redshift of the peak. To visualize the morphological changes in the nanoparticles, they were investigated with transmission electron microscopy (TEM).

The TEM images in figures 2.7a and 2.7b show the shape and size of the nanoparticles before and after etching with ferricyanide. They show that not only the size of the particles decreases but also the shape changes. Initially the particles have triangular or hexagonal prism shapes with sharp edges. After etching, the sharp edges are no longer present and the triangular and hexagonal prisms turn into round disk-like nanoparticles. A better representation of the size distribution, and the effect of ferricyanide on the particles, is shown in the histograms in figure 2.7c and 2.7d. The histograms show the size distribution of the nanoparticles before and after etching. They show that the size distribution shifts to smaller values after the particles are etched.

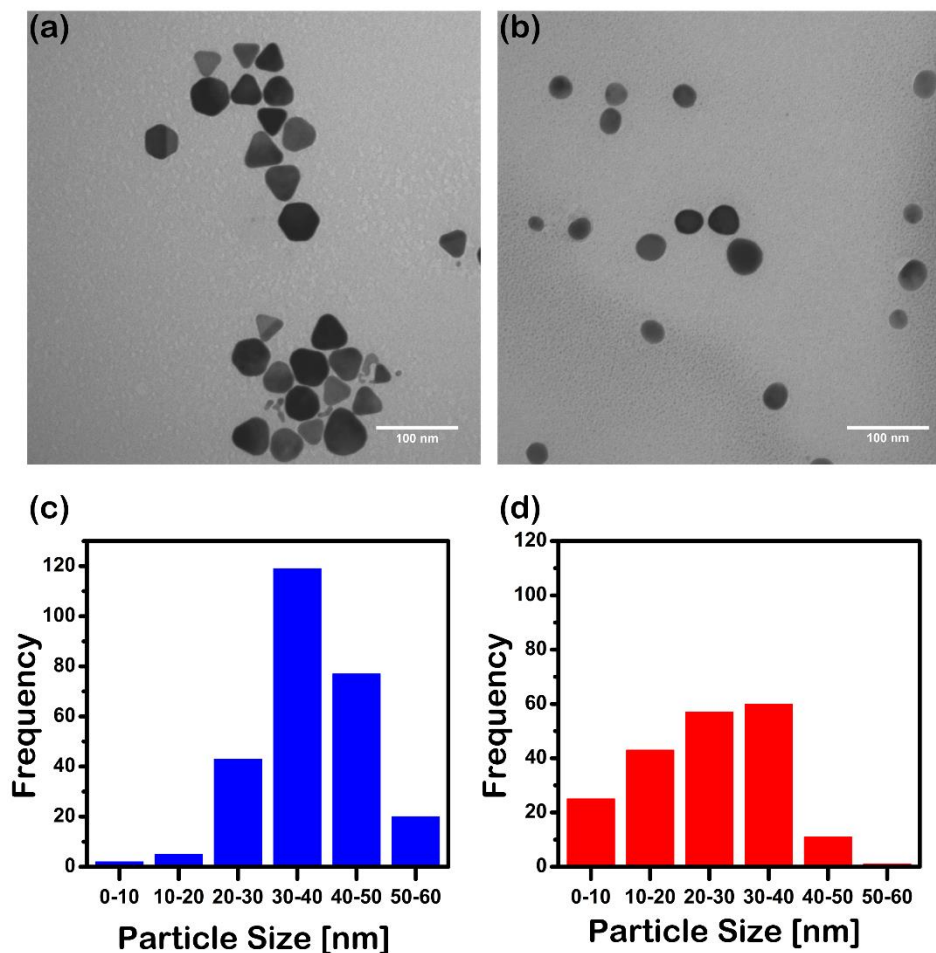


Figure 2.7. Transmission electron microscopy images before (a) and after (b) etching of the nanoparticles with ferricyanide. Particle size distribution before (c) and after (d) etching with ferricyanide. Morphological changes on the nanoparticles are observed upon incubation with ferricyanide.

The changes in the extinction spectra are therefore a result of morphological changes of the nanoparticles.

2.3.4 Adjusting Experimental Times

So far the etching of the nanoparticles took place over the course of 75 minutes with spectra being collected every 5 minutes. We noticed that the maximum difference in response, between a control platform (exposed to water) and target platform (exposed to quinine), occurs after approximately 2 minutes of etching. We hypothesized that the same colorimetric response can be observed in the initial stages of etching. Therefore the experimental setup was adapted to collect the spectra only during the first 10 minutes. The experiment in figure 2.8 shows results from the new experimental setup with ferricyanide as the etchant and PAH as the outermost layer installed on the film. Figures 2.8a and 2.8b show the etching spectra. They illustrate that the LSPR intensity of the control film (water) decays slower than the film with target. Figure 2.8c shows the normalized percent intensity decay of the control and the film incubated with quinine. The control sample reaches 15% in intensity decay at 6 minutes while the film with quinine reaches an intensity decay of 33%. These results show that the colorimetric response can be obtained with shorter

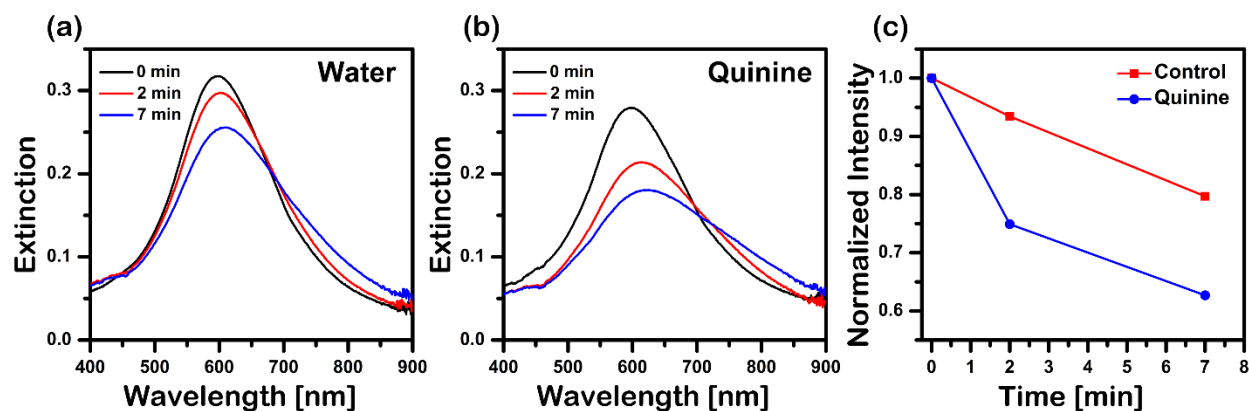


Figure 2.8. New experimental setup with ferricyanide and spectral collection over the course of seven minutes. Spectral decay during etching of films incubated with water (a) and quinine (b). (c) Normalized peak intensity decay plotted against time. Extent of intensity decay of quinine bound film is twofold greater than that of the control.

etching times and that the initial intensity decay can be monitored as the optical response. Also they display the successful adaptation of the platform to operate with ferricyanide.

2.3.5 Concentration dependence

To determine an effective concentration range, we studied the effect of quinine concentration on the polyelectrolyte aptamer film. We performed concentration dependence experiments. Six films were introduced to a range of concentrations of quinine, 0-500 μM . Figure 2.9 shows the spectral evolution of the extinction of the film over the course of 10 minutes during etching with the ferricyanide. The intensity of the films with no target and 50 μM (Figures 2.9a and b) decreases in a similar fashion. The intensity of films with higher concentration decreases to a greater extent (Figures 2.9c-e).

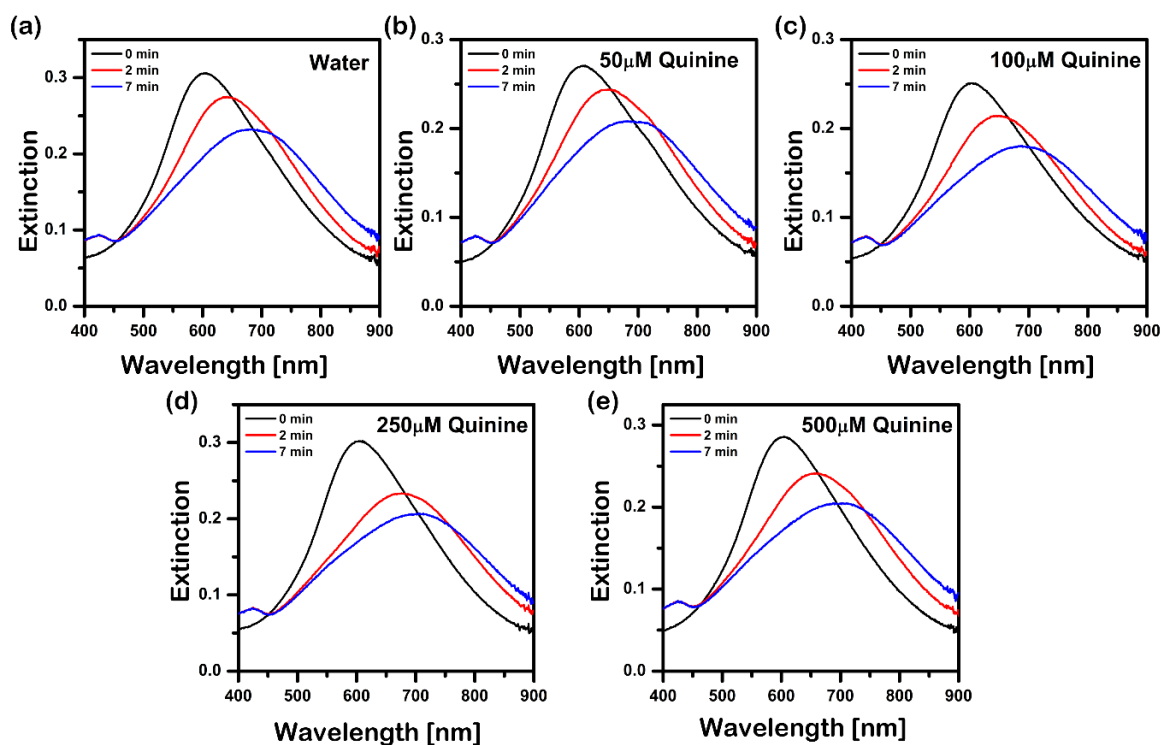


Figure 2.9. Concentration dependence experiments showing UV-visible spectra during etching in the first 10 min. Five films introduced to different concentrations of quinine ranging from 0-500 μM . The control and 50 μM (a) and (b), have similar LSPR decay while the higher concentrations(c)-(e) have greater peak decay.

A summary of six concentration dependence experiments is shown on figure 2.10. The percent intensity decay of the films with different conditions compared with the control. We obtain the data by extrapolating the percent intensity decay of the films in quinine when that of the control is ~15%. Results show a two fold increase in decay for the films in 250-500 μM quinine. In addition, this trend can be seen by naked eye in the inset in figure 2.10. The colour goes from blue (0 μM quinine) to a less intense bluish gray (250 μM). The results suggest that the effective working range of the platform is between 50 μM and 250 μM . These experiments were all done in water without potential interfering species. The next stage is to test a range of ions which could interfere with the polyelectrolyte-aptamer film and disrupt the colorimetric response.

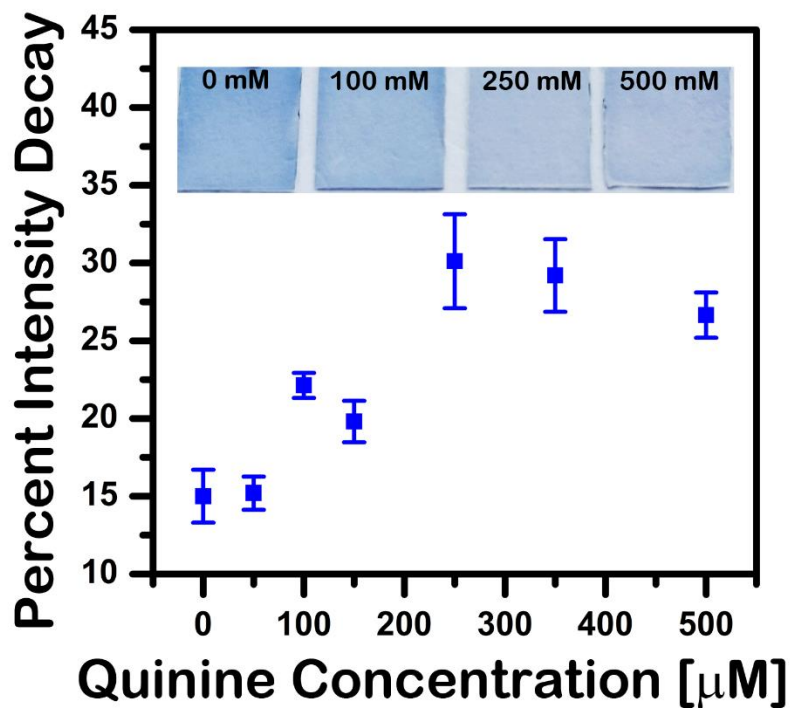


Figure 2.10. Effect of quinine on the permeability of polyelectrolyte-aptamer films. Effect of quinine is monitored as percent intensity decay of the LSPR of nanoparticles. Individual films were incubated in different concentrations of quinine. An average of six independent experiments, with SEM as error bars, shows a two fold increase in colorimetric response with increasing quinine concentration. (Inset) Visual colorimetric response.

2.3.6 Ionic interference

Investigation of possible interfering species determines whether or not a sensing platform can operate in complex media. Platforms that provide rapid results from complex media are highly desirable because they can be used in field analysis where sample preparation is not vital. After establishing an effective concentration range, we investigated the sensing performance under a variety of ions. Electrostatic interactions which hold together the polyelectrolyte aptamer film can be disrupted by charged species so an ion interference study was necessary.^{[67] [14]} Based on interactions between polyelectrolyte and ions, the platforms have been studied for nanofiltration

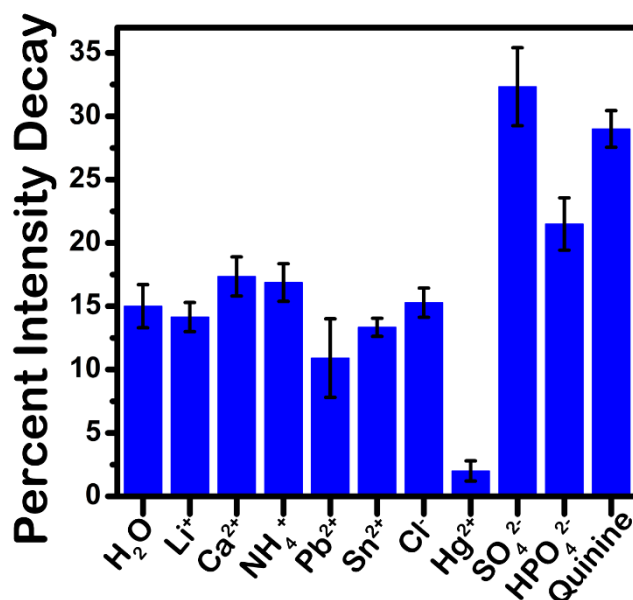


Figure 2.11. Percent intensity decay of LSPR of the platform in the presence of various ions compared with that of water and quinine. Sulfate and Mercury (II) ions interfere with the platform but the rest of the ions show no significant effect. Six independent experiments performed with the exception of Hg²⁺, Sn²⁺, Pb²⁺ (N=3). Error bars are SEM.

membranes.^[68] Therefore, it is important to determine and understand possible interactions between ions and the polyelectrolyte films. In addition to metal ions and common anions, we also tested some heavy metal ions (Hg²⁺, Sn²⁺, Pb²⁺) because of their known interactions with

DNA.^{[69],[70],[71]} To study the colorimetric response, we incubated the platforms with various ions and obtained the percent intensity decay for each of the conditions. Figure 2.11 shows a summary of the ion interference experiments with the concentration of ions being 500 μM .

Monovalent and divalent cations, together with chloride, have virtually no effect on the film. The response of the films in phosphate is slightly higher than that of the control, while the intensity decay of the film in sulfate ions is the same as that of the quinine films. The Pb^{2+} and the Sn^{2+} had no effect on the DNA. On the other hand, mercury ions significantly influenced the etching of the nanoparticles. Sulfate ions interfered with the platform as well producing a false positive response. The interference of mercury and sulfate was further investigated to pinpoint their role in the disruption of the colorimetric response.

2.3.6.1 Interference of Mercury (II)

The intensity decay of the films incubated in Hg^{2+} is very small compared to the control. The absence of etching is not due to the interaction of mercury with the polyelectrolyte-aptamer film but with the nanoparticles underneath. This interaction seems to make the nanoparticles inert to etching and the platform does not generate a colorimetric response. The absence of changes in the plasmonic signal of the film which was exposed to mercury (II) ions, can be due to the displacement of silver by the Hg^{2+} ions^[72] in the nanoparticles. This displacement hinders the etching process. Figure 2.12 shows the effect of mercury (II) chloride on the LSPR of the nanoparticles. The original particles have an LSPR peak at 580 nm with an extinction intensity of 0.49. Following the incubation with mercury (II) ions, the peak intensity dropped to 0.36 and the peak position blueshifted to 560 nm. The decrease in intensity and the blue shift suggest a change in morphology of the nanoparticles and some chemical reaction of Ag with Hg^{2+} . It has been

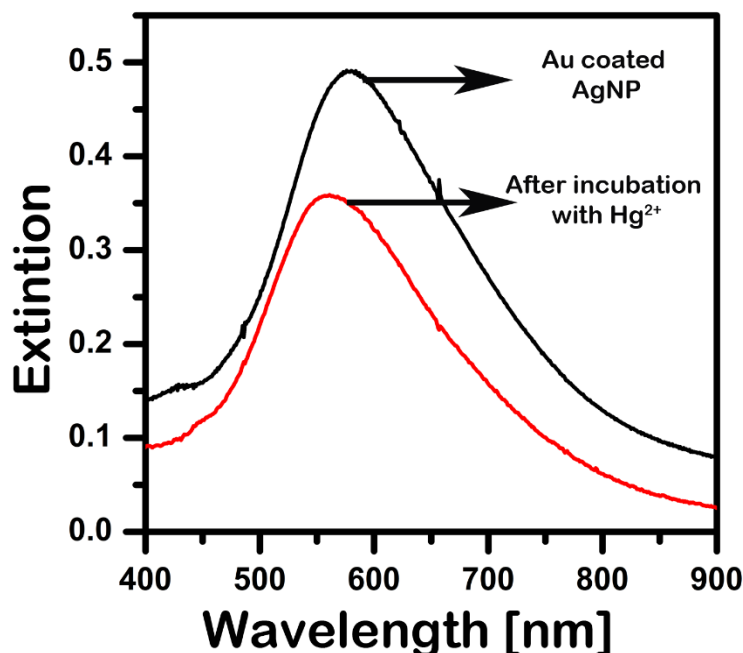


Figure 2.12. Effect of mercury on the nanoparticles monitored via LSPR. LSPR peak decreases in intensity and blue shifts upon incubation with mercury (II) ions.

reported that the mercury (II) ions can dissolve or displace silver atoms [72-73]. We performed Energy Dispersive X-ray measurements to check for the displacement of silver by mercury. Figure 2.13 show the EDX spectra of original as-synthesised particles (Figure 2.13a) and particles incubated with mercury (Figure 2.13b). Due to the very similar values M_{α} values for gold and mercury, 2.120 and 2.195 respectively, the peaks could not be distinguished and relative amounts of gold and mercury could not be accurately quantified. However qualitative conclusions can be

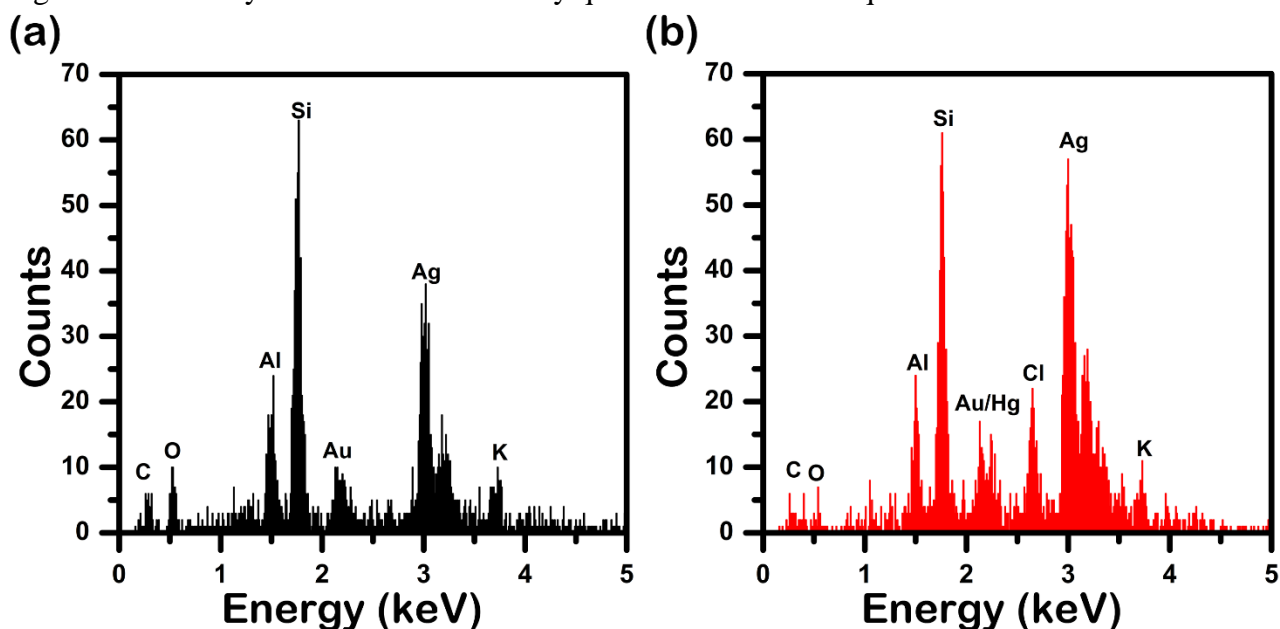


Figure 2.13. EDX spectra of nanoparticles incubated with and without mercury. (a) Spectra of as-synthesized gold-coated silver nanoparticles. (b) Spectra of gold coated silver nanoparticles after incubation with 1 mM mercury (II) chloride.

drawn. Figure 2.13a shows a gold peak around 2.12 keV. In figure 2.13b the gold peak contains a shoulder which could signify the presence of mercury. In addition after the incubation with mercury(II) chloride, we detected a chloride peak at 2.66 keV. The presence of this peak suggests oxidized silver ions on the surface of the nanoparticles, likely in the form of AgCl. Also, if mercury (II) deposits as mercury(0) on the nanoparticles, the high vacuum needed to perform EDX could cause the mercury to evaporate, making it hard to detect.

2.3.6.2 Interference of Sulfate

The response of the platform incubated with sulfate is very similar to the response of the platform incubated with quinine. These results could mean that sulfate ions are interacting with the polyelectrolyte-aptamer film to enhance the diffusion of ferricyanide ions or with the nanoparticles to increase their etching rate. To determine the effect of sulfate ions on the nanoparticles the etching was done on gold-coated silver nanoprisms immobilized on glass substrate without the polyelectrolyte overlayer. One substrate was kept in water and the other in 1 mM sulfate. Figure 2.14 shows the etching spectra over the course of 25 minutes and the negligible difference between the two samples. Hence we conclude that sulfate does not play a role on the etching of the nanoparticles and the interaction of sulfate with the polyelectrolyte-aptamer film likely resulted in the false positive response.

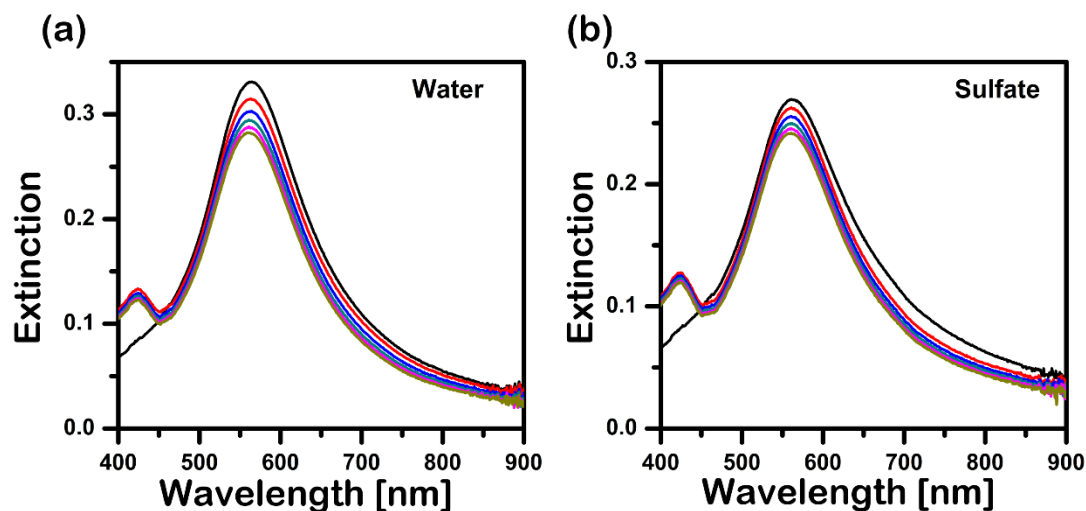


Figure 2.14. Etching of nanoparticles in the presence of water and sulfate. The presence of sulfate ion does not interfere with the etching process.

To investigate whether the sulfate ions interact with the polyelectrolyte, i.e. PAH/PSS, or the DNA-aptamer incorporated in the film, we monitored the LSPR change of samples consisting of PAH/PSS only, or with a random DNA sequences. We replaced the aptamer with random DNA1

for one film and a longer strand, random DNA2, for the other. Following incubation with 500 μM sodium sulfate, the films are placed in ferricyanide. Figure 2.15 shows that the sulfate gives a false positive response in all three platforms when compared with the control. The corresponding films incubated in water had an average of 15% intensity decay while the films with PAH/PSS, PAH/Random1 and PAH/Random2 incubated in Na_2SO_4 had 26%, 30%, and 38.7% intensity decay respectively. From these results, we conclude that sulfate ions interact with the polyelectrolyte film and not with the DNA aptamer.

A potential explanation for the interference of sulfate, is the charge on and the resemblance to the charged groups present on the film. Sulfate ions are similar to the sulfonate functional groups

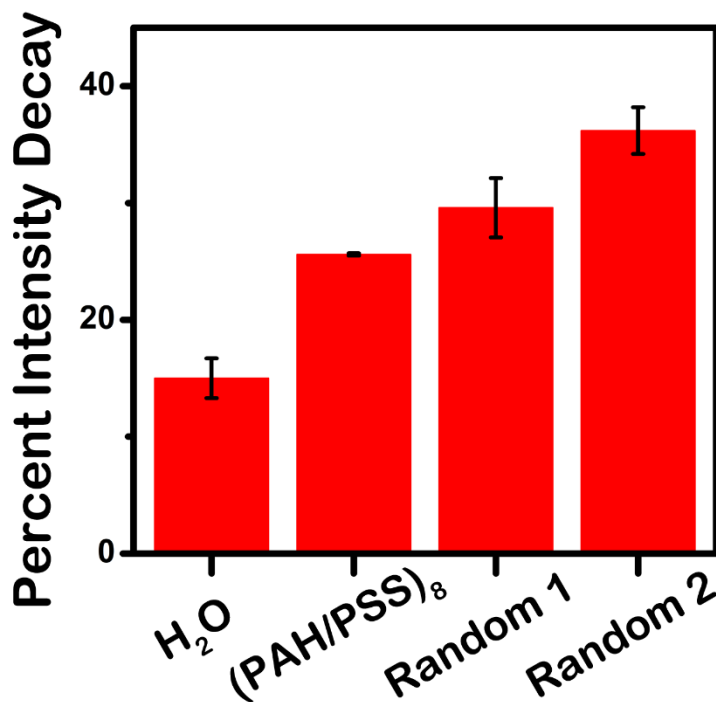


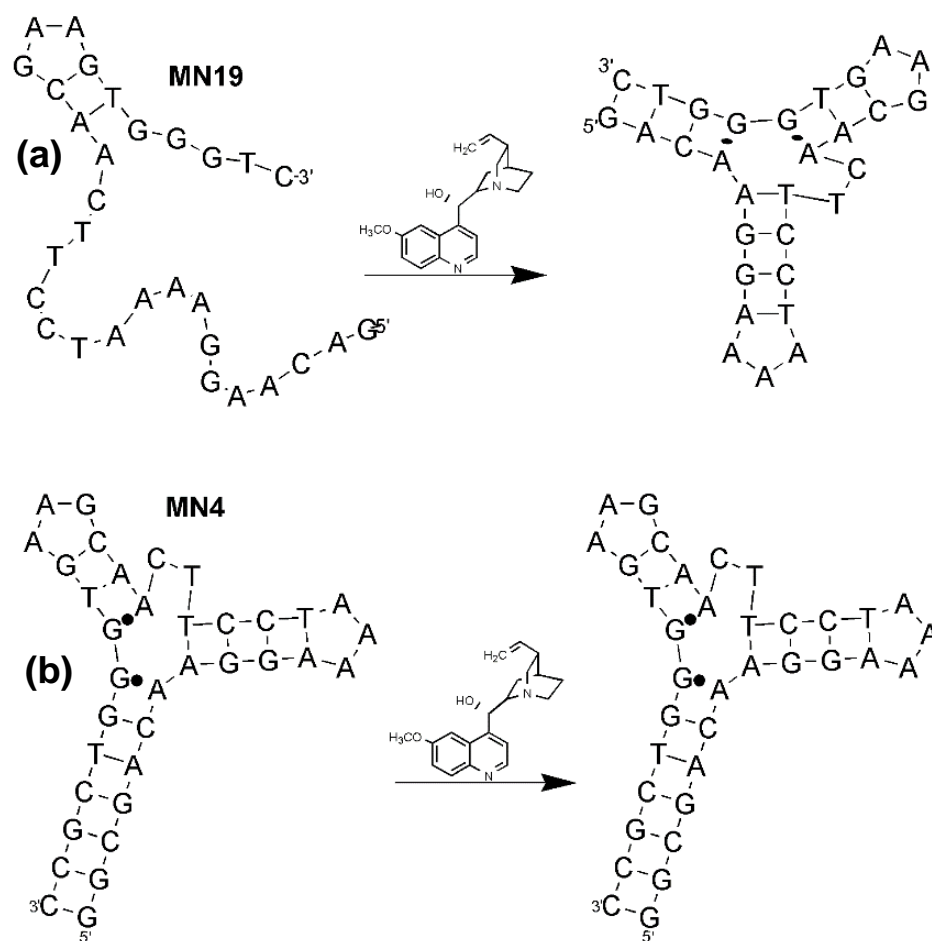
Figure 2.15. Control experiment for the determination of sulfate interference. Platform was tested by replacing the MN19 aptamer by polyelectrolyte (PSS), Random DNA1, and Random DNA2. Results show that sulfate ions interfere in all three modifications of the film. Three independent experiments for each condition with SEM as error bars.

in the PSS polyelectrolyte, which is part of the film. During incubation, the sulfate ions could interact with the ammonium groups in PAH-PSS interaction sites interaction.^[74] Due to the 2-charge on the ions, one sulfate ion could interact with two protonated amine groups in the PAH. This interaction might cause structural changes in the film leading to greater permeability. In addition, the sulfate ions lie on the kosmotropic end of the Hofmeister series. Hofmeister series ranks ions based on their interactions with the surrounding water molecules.^[15] Kosmotropic ions are highly hydrated and lead to the formation of hydrogen bonding networks.^[54a] When sulfate ions penetrate the film, they may alter the water structure in it. This effect which could lead to rearrangement of the film, enhancing the permeability. The effect of sulfate can be remediated by precipitating it with BaCl₂ prior to testing (See section 3.3.5). After establishing that mercury (II) and sulfate ions interfered with the platform, the next step was to investigate the effect of the conformational changes of the aptamer and their role on the film.

2.3.7 Effect of Aptamer Folding on the Permeability of the Film

The colorimetric response of our platform results from the target binding to its corresponding aptamer incorporated in the film. The binding of the aptamer induces a change in the polyelectrolyte-aptamer film and its permeability increases. The increase in permeability leads to greater diffusion of the etchant molecules and therefore greater etching with the binding of the target. To investigate whether a structural change in the aptamer is necessary for the platform to work, we use MN4 aptamer. The MN4 aptamer is identical to MN19 however it has an additional three base pairs on stem one. These three added base pairs allow for more stability and the secondary structure consisting of the three-stem junction forms prior to binding. Unlike the MN19 aptamer where the binding of the target induces a three stem junction to form, the MN4 aptamer does not change its conformation when binding to cocaine or quinine^[75]. The difference between the aptamers is illustrated in scheme 2.2. The binding sites for quinine are identical and the dissociation constants (K_D) for the MN19 and the MN4 are $0.7 \pm 0.02 \mu\text{M}$ and $0.23 \pm 0.03 \mu\text{M}$ respectively.^[76] The similar K_D values make these aptamers a great tool to investigate our target responsive film.

Films were built with the MN4 aptamer instead of the MN19 and the experiments were carried out the same way. Following the etching, the peak intensities were then obtained and normalized. Results show very little difference between the films incubated in water and in 250 μ M quinine. Figure 2.16 shows the very similar intensity decays between the two conditions. After



Scheme 2.2. (a) Quinine binding aptamer MN19 folds upon binding to its target, quinine. (b) Quinine binding aptamer MN4 has a preformed secondary structure and does not change its conformation upon binding to quinine.

two minutes, the intensity decay for the film incubated in water is 11%, and 13.3% for the film incubated in quinine. These results show that the absence of the structural change in the MN4 aptamer does not allow a colorimetric signal to be generated.

Therefore, a structural change in the MN19 aptamer is crucial for the functionality of the platform. The platform with the MN4 aptamer cannot distinguish between target and the absence of target. The similar responses between the two conditions could mean one of two things. First, the target (quinine) is binding to the aptamer but the lack of structural change of the MN4 aptamer does not have an effect on the diffusion of the etchant. The other possibility is that the quinine cannot bind to the MN4 aptamer and therefore does not generate a response. Due to the high similarity of the aptamers, the more likely scenario is that quinine binds but there is no response. In the future, if the platform needs to be adapted for other analytes, the aptamers incorporated in the film must undergo structural changes upon binding.

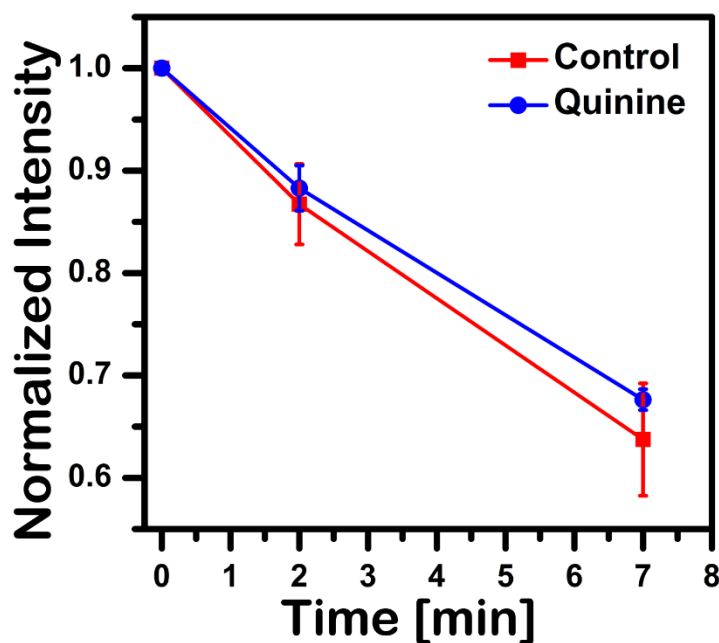


Figure 2.16. Normalized intensity decay of nanoparticles in a platform where MN19 was replaced with MN4 aptamer. The absence of a structural change in the MN4 aptamer results in almost identical intensity decay between control (water) and target bound film (quinine). The graph shows three independent experiments with SEM as error bars.

2.4 Conclusions

In summary, we successfully replaced the sulforhodamine B aptamer with the cocaine/quinine binding aptamer. Reproducibility of the experiments has been improved by using ferricyanide ions as the oxidizing agents instead of the iodide/triiodide couple. An outer layer of PAH had to be installed for the film to work with ferricyanide. Concentration dependence show an effective detection range between 50 and 250 μM of quinine; while the interfering species were determined to be mercury (II) ions and sulfate ions. It was established that mercury (II) ions interact with the nanoparticles while sulfate ions interact with the polyelectrolyte film to generate false positive responses. Other monovalent and divalent anions and cations, including heavy metal ions, did not interfere with the platform. Variations of the aptamer also shows that the aptamer must undergo a structural change for the permeability of the film to increase to generate the colorimetric response.

We achieved morphology based optical sensing using the change in permeability of polyelectrolyte aptamer films. Simply replacing the aptamer without modifying the procedure indicates the versatility of the films. Also, this method of sensing is label free, and the signals are assessable by naked eye. Challenges with the consistency of batch-to-batch synthesis of nanoparticles led to variations of results. Therefore, the films were characterized using cyclic voltammometry for more quantitative and reproducible outcomes.

CHAPTER 3: Modifying Electrodes with Polyelectrolyte-aptamer Film for Electrochemical Sensing

3.1 Introduction

3.1.1 Towards Miniature Electrochemical Systems

Small electrochemical systems for microscale investigation means low cost, on-site and in-situ analysis. The advantage of electrochemistry is that the components can be miniaturized without effecting their functionalities.^[77] Portable systems are highly desirable because they provide rapid results in a cost effective way when compared with traditional laboratory instrumentation. Smaller sample sizes result faster analysis and rapid diagnosis. These systems have great potential for applications in environmental testing, health monitoring, and military use.^{[78] [78b]}

The material has great impact on the performance of electrochemical systems, especially the electrodes. Mercury was the prime choice for working electrodes due to the smooth surface.^[79] However due to facile surface modification methods, gold electrodes have been used for the study of polyelectrolyte films. Gold provides a flat surface where these films can deposit uniformly.^[80] Another material that can be used as a working electrode is Indium Tin Oxide (ITO). Typically, indium oxide is doped with tin oxide in a ratio of 9:1.^[81] ITO coated glass is easily available and can be patterned using chemical etching or laser printing. The surface of the ITO can be activated through various methods such as RCA bath or plasma cleaning. The activation allows for facile modification of the electrodes.^[82] In addition, the ITO is transparent and can be utilized for simultaneous optical and electrochemical investigation. In this work modified ITO working electrodes will be used for electrochemical investigation.

3.1.2 Electrochemistry and Cyclic Voltammetry

Electrochemical sensors are user friendly, and can provide rapid quantitative results. In the electrochemical sensors, the recognition element is typically assembled on the transducer, which is the electrode. The electrochemical signal could be a change in the potential, current, or impedance of the electrode. Typically, in electrochemical sensing, the redox active species are immobilized on the surface of the electrode or on a recognition element such as an aptamer. The advantage for using LbL polyelectrolyte-aptamer films is that the redox active species, ferricyanide, remains the same and is not linked with the analyte or the film. This method is label-free and requires no chemical modifications.

Herein, the method chosen to investigate the target responsive films is cyclic voltammetry. Cyclic voltammetry is a technique where the potential on an electrode is scanned with respect to a reference electrode. The system consists of three electrodes: working electrode, reference electrode and counter electrode. The role of the reference electrode is to provide stable potential to which the potential of the working electrode can be scanned.^[83] The counter electrode is used to complete the circuit. The working electrode is where the reaction of interest takes place. The three electrodes are immersed in a solution containing a redox active species in a supporting electrolyte (KCl). As the potential is scanned the redox active species $[\text{Fe}(\text{CN})_6^{3-}/\text{Fe}(\text{CN})_6^{4-}]$ is oxidized or reduced, at the working electrode, depending on the direction of the scan. The role of the supporting electrolyte (KCl) is to reduce the migration of the ions to the opposite electrode. As the voltage is scanned the redox of $\text{Fe}(\text{CN})_6^{3-}/\text{Fe}(\text{CN})_6^{4-}$ gives rise to excitation signals which correspond to currents arising from oxidation or reduction. The peak currents (equation 3.1) depend on scan rate(v), diffusion coefficient (D), electrode area(A), concentration(c) and number of electrons(n) being transferred.^[84]

$$i = 2.686 \times 10^5 n^{3/2} A c D^{1/2} \nu^{1/2} \quad (3.1)$$

Cyclic voltammetry has been used for the study of the polyelectrolyte multilayers though not on polyelectrolyte-aptamer films. This method can provide information on the diffusion of ions through the film, swelling, and permeability.^[85] It was used to study the permeability and stability of polyelectrolyte films,^{[86] [86b] [74]} and to investigate the properties of pH-switchable ultrathin membranes.^[68]

3.1.3 Objective

In this work, we used cyclic voltammetry to shed light on the properties of the polyelectrolyte-aptamer film with and without target. The working electrodes were modified with polyelectrolyte-aptamer films and peak currents were monitored to explore the rate of diffusion of ions. Electrochemical characterization of the platform was performed with the target-responsive film assembled on an Indium Tin Oxide (ITO) electrode. The peak currents were measured before and after target binding. One of the main goals of using electrochemistry was to corroborate the findings with the colorimetric platform for the determination interfering species and a concentration range. Additionally, we investigated the effect of the aptamer folding by using films comprising of two versions of the aptamer, MN4 and MN19.

Cyclic voltammetry provides information whether our platform has the potential for development as an electrochemical sensor. The electrochemical sensor would provide a more quantitative response but with the drawback of having to use instrumentation. On the other hand, the colorimetric method is less quantitative but visually assessable. Further development and characterization of polyelectrolyte-aptamer films will shed light on new approaches in aptamer-based sensing.

3.2 Experimental

3.2.1 Preparation and Modification of Electrodes

Indium Tin Oxide (ITO) coated glass was obtained from data technologies. The ITO covered microscope slide was patterned using Versa Laser. The size of the electrodes was 3 mm in diameter. They were rinsed and sonicated for 10 minutes in acetone to remove any organic residues from the surface. After sonication, they were placed in RCA bath for 15 minutes at 80 °C. This step provides further cleaning and activation of the surface.

Solutions of PAH and PSS with concentrations of 2 mg/mL in 0.2 M NaCl were prepared. After RCA bath, the electrodes were placed in the robotic dipper. For one bilayer, the electrodes were first dipped in the PAH solution for 10 minutes followed by two rinsing steps. The same was done for the deposition of PSS. This process was repeated four times to deposit the base bilayers. The negatively charged polyelectrolyte, PSS, was then replaced with a solution containing the MN19 aptamer. The concentration of the aptamer was 5 μ M in 1x PBS. The same deposition procedure was followed to deposit another eight bilayers of PAH/DNA. The film was then dipped in the PAH solution to put a final positively charged cap.

3.2.2 Electrochemical Measurements

The modified electrodes were placed in \sim 7 mL solution of 60 μ M $K_3Fe(CN)_6$ in 6 mM KCl with a platinum wire counter electrode and a Ag/AgCl reference electrode. Cyclic voltammetry was performed for as-deposited electrodes. The potential was scanned from -0.35 V to +0.7 V with a scan rate of 0.1 V/s. After, the electrodes to be used as control experiments were incubated in water and the ones to be used with target were incubated in 250 μ M or 350 μ M quinine for 30 min. Following the incubation, cyclic voltammetry was performed again. The anodic peak

currents were extrapolated from before and after target binding and their difference ($\Delta I_{p,a}$) was determined to be the electrochemical signal.

3.2.3 Concentration Dependence and Ionic Interference

Cyclic voltammetry was performed to investigate concentration dependence. Scans were taken on six individual electrodes before and after immersion with varying concentrations of quinine. The quinine concentrations used were 0 μM , 50 μM , 150 μM , 250 μM , 350 μM , 500 μM . The $\Delta I_{p,a}$ of each condition was obtained and plotted. Similarly, the same procedure was followed for the ion interference experiments. The following salts with concentration of 1 mM were tested: MgCl_2 , MgSO_4 , NaHPO_4 , NH_4Cl , LiCl , PbCl_2 , HgCl_2 , SnCl_2 . For interfering species such as sulfate ions, they were removed from the solution by precipitation with BaCl_2 . Fresh, as-deposited electrodes had initial scans taken and placed in solution where the amount of sulfate ions was reduced. Scans were taken again after incubation and $\Delta I_{p,a}$ was obtained.

3.2.4 Non-specific binding

Ecgonine hydrochloride is a cocaine metabolite which does not bind to the MN19 aptamer and is present in both quinine and cocaine. It was used as a nonbinding molecule to investigate if the MN19 aptamer binds non-specifically. Similar to previous experiments the modified electrodes were incubated with ecgonine and cyclic voltammetry was performed before and after immersion. Additionally, the MN19 was replaced with a random strand of DNA (DNA-210 5'-CTG TGC GTG TGA CAG CGG CTG A -3'). This experiment tests whether the quinine molecule binds non-specifically to the polyelectrolyte-DNA film.

3.2.5 Optimization

First, the number of PAH/PSS base bilayers were varied to determine the optimal amount needed for the difference in electrochemical signal to be generated. The number of PAH/PSS bilayers was increased from zero to four while keeping the number of PAH/DNA the same. Cyclic voltammetry was performed on five electrodes with varying numbers of PAH/PSS before and after incubation with the target. The anodic peak currents, $I_{p,a}$, were compared. The number of PAH/DNA bilayers was also optimized. Three platforms were tested with 4, 8, and 12 bilayers of PAH/DNA while keeping everything else the same. Similar to previous experiments, cyclic voltammetry was performed with and without target. The $\Delta I_{p,a}$ was obtained and plotted against the number of bilayers.

3.2.6 Aptamer Folding

There are two versions of the cocaine/quinine binding aptamer. MN19 aptamer folds upon binding to the target while the MN4 does not change structure upon binding.^[87] The effect of aptamer folding was investigated by comparing the electrochemical response, $\Delta I_{p,a}$, of modified electrodes with MN19 aptamer and with MN4 aptamer. Two electrodes were prepared with MN19 aptamer. One served as the control and the other was incubated with the target. The same procedure was followed with the MN4 aptamer. The $\Delta I_{p,a}$ was compared between the control and target conditions of the same aptamer, but also between the films with the different aptamer.

3.3 Results and Discussion

3.3.1 Effect of Base Bilayers

Because the colorimetric characterization monitors the diffusion of ferricyanide by observing the etching of the nanoparticles, a more quantitative method was necessary to better understand the diffusion of the etchant through the film. We first examined the composition of the film required for the electrochemical platform by varying the number of PAH/PSS bilayers without changing the PAH/Aptamer. A typical cyclic voltammogram is shown in Figure 3.1a. Figure 3.1b

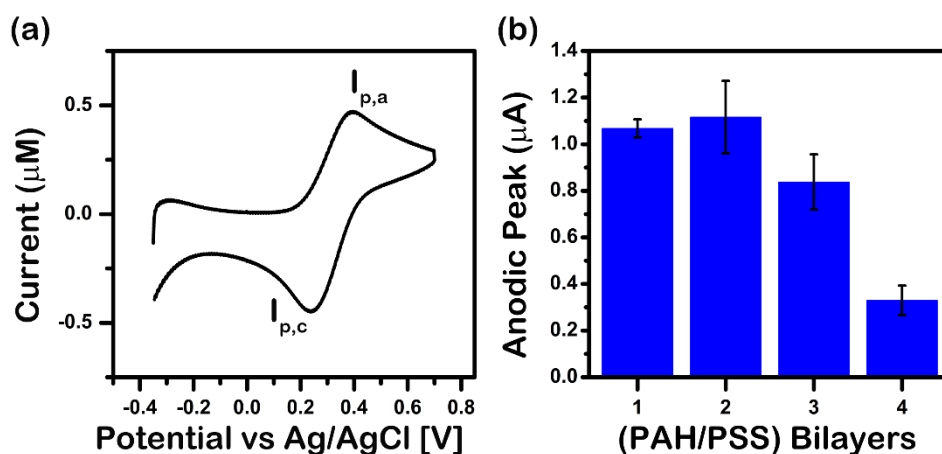


Figure 3.1. (a) Typical cyclic voltammogram of an ITO electrode covered with polyelectrolyte-aptamer film. (b) Anodic peak currents of cyclic voltammograms of electrodes covered with different number of bilayers of PAH /PSS. Increasing number of bilayers means greater surface coverage and a lower peak current. Potential is scanned from -0.35V to $+0.7\text{V}$ vs Ag/AgCl. Concentration of ferricyanide is $60\mu\text{M}$ in 6mM KCl and the scan rate is 100mV/s . Triplicate experiments were performed with SEM as error bars.

shows the anodic peak currents vs the number of base bilayers; a decrease in anodic peak current is observed with increasing number of bilayers. The first two bilayers installed have similar peak currents. A drastic drop in peak current follows with the installation of the fourth bilayer. This finding is consistent with the literature where researchers noted that the polyelectrolytes deposit as coils during the layer by layer assembly, and the first two bilayers generate films that are porous.^[86b] The peak currents then arise from the redox reactions occurring at exposed areas of the electrode, which have similar magnitude as the bare electrode ($0.82 \pm 0.13 \mu\text{A}$). Upon the

installation of the third bilayer, a sharp decrease in peak currents was observed suggesting a more even coverage of the polyelectrolyte on ITO. The change in peak current suggests that a minimum of four bilayers are needed for a significant coverage of the electrode.

3.3.2 Concentration Dependence

The effect of quinine on the film is obtained by monitoring the difference in anodic peak currents ($\Delta I_{p,a}$) before and after binding. Polyelectrolyte-aptamer films are assembled on ITO electrodes and control and target binding experiments are performed. Initially we compare two conditions, control (in water) and quinine (350 μM). Results show a greater $\Delta I_{p,a}$ for the quinine film than the control. Figures 3.2a and 3.2b show cyclic voltammograms before and after target binding for typical electrodes. The peak currents from the scans before target binding are in the

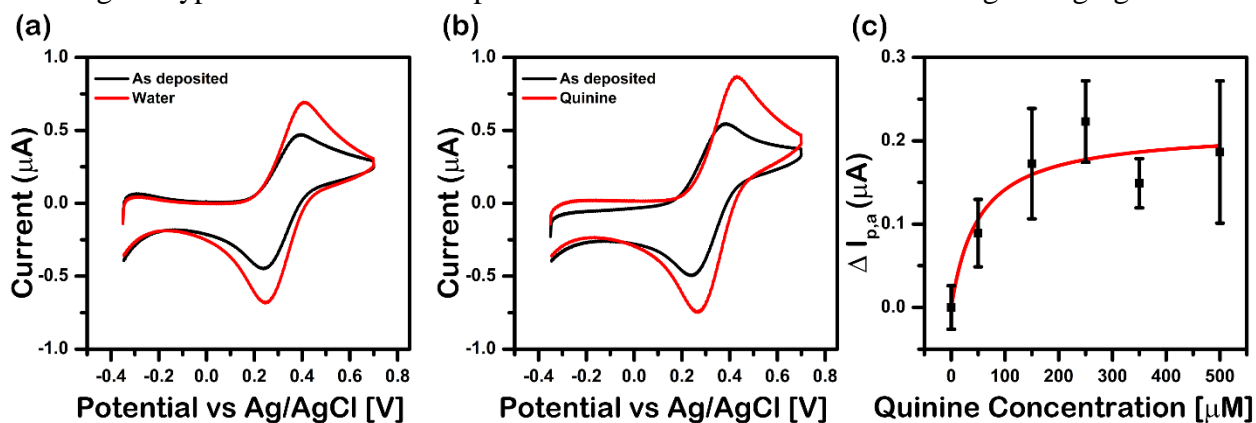


Figure 3.2 . Representative voltammograms of films on ITO electrode of 60 μM potassium ferricyanide in 6 mM KCl at a scan rate of 100mV/s. (a) &(b) Voltammograms taken after incubation with the target (red line) line had higher anodic peak currents than voltammograms taken prior to incubation(black line). (c) The change in anodic peak current ($\Delta I_{p,a}$) obtained and plotted against increasing concentrations of quinine. The change in anodic peak current increases with increasing concentration of quinine with a saturation point at 200 μM .(N=15 for 0 μM an 350 μM and N=4 for 50,150,250 and 500 μM) Error bars are SEM.

range of 0.2-0.5 μA . After incubation, the peaks of both control (immersed in water) and target experiments (immersed in quinine) show an increase in peak currents. The increase in peak currents imply an increase in permeability of the film. This increase is higher for the electrodes exposed to the target (quinine) than the electrodes exposed to water, suggesting that quinine has

an effect on the film. The binding of quinine to the aptamer in the films enhances the films permeability, which gives rise to higher peak currents.

Once the difference between control and target conditions was established concentration dependence experiments were performed. Figure 3.2c shows the change in anodic peak current for the increasing concentrations of quinine. Similar to the etching experiments, the effect of quinine on the film is significant. Figure 3.2c shows the concentration range 0 to 500 μM . Again, the data points are obtained by taking the difference in the anodic peak current from before and after target binding and averaging them. The control films incubated in water have the smallest $\Delta I_{p,a}$. The effect of quinine then increases with concentration. Before target binding the electrodes, modified with polyelectrolyte-aptamer film, have similar anodic peak currents, ranging from 0.2 μA to 0.5 μA . Reproducible results are obtained when the initial anodic peak currents are in the aforementioned range. Also, the initial peak currents can serve as indicators to establish the quality of the films. After incubation, the anodic peak currents increase. The responses from the concentration dependence experiments are fitted to determine the dissociation constant of the aptamer on the film. The one-site Langmuir binding model (Equation 3.2) is used with the assumption of 1:1 ratio between aptamer and quinine. $\Delta I_{p,a}$ is the signal associated with specific binding with B_{max} representing the maximum signal. K_D is the dissociation constant and X is the concentration of quinine in micromolar.

$$\Delta I_{pa} = B_{\text{max}} \frac{X}{K_D + X} \quad (3.2)$$

The dissociation constant for the MN19 aptamer incorporated in the film is $56.16 \pm 18.2 \mu\text{M}$. This value is about two orders of magnitude higher than the dissociation constant of the aptamer in solution ($K_D = 0.70 \pm 0.02 \mu\text{M}$).^[76] The reason for the higher K_D value is a result of the

incorporation of the aptamer in the film. The added interaction of the aptamer with the polyelectrolyte film hinders the binding of the aptamer to quinine.^[63]

3.3.3 Specificity of Detection

Species that do not bind to the aptamer can possibly interact with the platform in other ways to give false positive responses. To test the specificity of the platform, we use the ecgonine molecule, a major cocaine metabolite, as control. Ecgonine HCl is a bicyclic ring and does not bind to the MN19 aptamer.^[88] The response of the platforms incubated with water (control) and quinine are compared with the response of the platform incubated with 350 μM ecgonine HCl. Figure 3.3 shows that ecgonine does not interact with the platform. The $\Delta I_{p,a}$ for the control and ecgonine are $0.19 \pm 0.03 \mu\text{A}$ and $0.22 \pm 0.05 \mu\text{A}$ respectively, while that of the platform exposed to the target is $0.42 \pm 0.05 \mu\text{A}$. The response of the sensor incubated with ecgonine is comparable to control. Therefore exposure to ecgonine does not lead to false positive results.

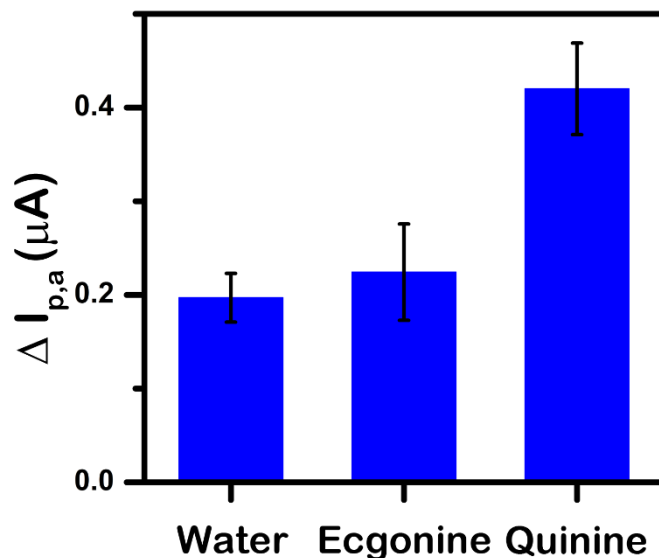


Figure 3.3. $\Delta I_{p,a}$ of ecgonine compared with those of quinine and water. The response of ecgonine is similar to that of water suggesting no interaction with the aptamer. N=15 for water and quinine and N=3 for Ecgonine with SEM as error bars.

Next we confirmed that the response of the platform comes from binding of the quinine to the aptamer in the film, and not some non-specific interaction with the polyelectrolytes, by substituting the aptamer with a random strand of DNA. Figure 3.4 shows that when the random DNA is incorporated in the film instead of the MN19 aptamer, the $\Delta I_{p,a}$ between the platforms incubated in water and quinine are very similar, $0.15 \pm 0.03 \mu\text{A}$ and $0.09 \pm 0.05 \mu\text{A}$. It suggests that quinine does not interact with the film without MN19. These results show that the quinine binds only to the MN19 aptamer to generate a response.

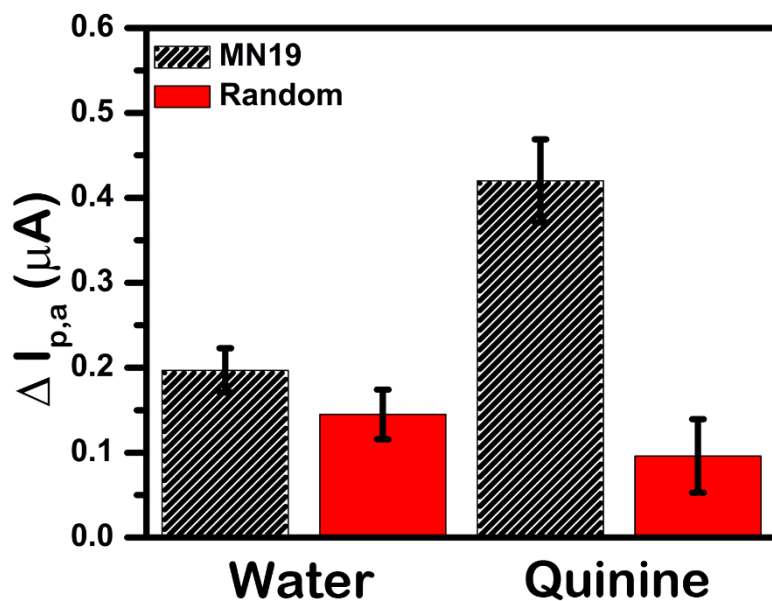


Figure 3.4. The effect of quinine on a random DNA oligonucleotide incorporated on the film. (Red) $\Delta I_{p,a}$ of quinine when MN19 aptamer is used. (Striped) $\Delta I_{p,a}$ of quinine when random DNA1 is used. Response of the platform when a random DNA is used is comparable to that of the control. Experiments with random DNA were done in triplicate. SEM was used for error bars.

3.3.4 Optimization

Experiments to maximize the response of the platform were performed by monitoring the anodic peak current of electrodes incubated in water and quinine prior to cyclic voltammetry scans. The number of base bilayers (PAH/PSS) was varied from one to four while keeping the (PAH/DNA-aptamer) bilayers unchanged. The maximum response was observed when four bilayers are installed (Figure 3.5). The anodic peak currents between control (water) and quinine-bound films are comparable when 0-3 bilayers are installed. A significant change of $0.98 \pm 0.05 \mu\text{A}$ in anodic peak current is observed upon the installation of the fourth bilayer. These results show that at least four bilayers of PAH/PSS are required for a functional polyelectrolyte-aptamer film. The variation in response for the first and second bilayers arise due to the non-uniformity of ITO surface and uneven deposition. [86a, 89] The uneven surface of the ITO contributes to the

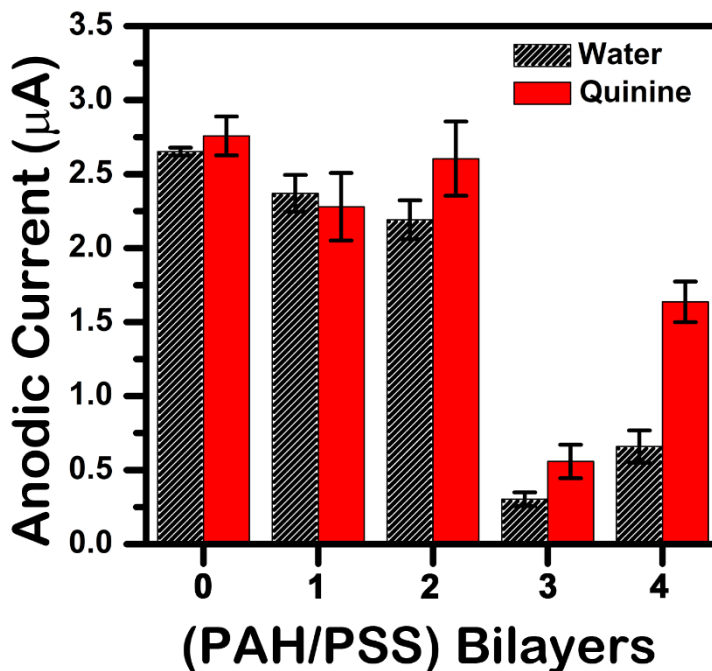


Figure 3.5. Response of platform in varying bilayers of PAH/PSS with the PAH/DNA-aptamer on top. Anodic peak currents of separate electrodes previously incubated in water followed by quinine. The anodic peak currents are comparable for the first three bilayers but a significant increase occurs in with four bilayers. Experiments were done in triplicate with SEM as error bars.

variation in anodic peak currents obtained from electrodes therefore the greatest difference between the two conditions occurs with four bilayers installed. The importance of having four bilayers of PAH/PSS could lie in their role on the formation of the PAH/DNA layers on top. Four bilayers of PAH/PSS may provide a uniform surface charge and consistency for ideal deposition of the PAH/DNA bilayers.

To investigate the effect of the amount of aptamer on the film, the bilayers of PAH/DNA were varied and cyclic voltammetry was performed. The number of bilayers tested was 4, 8, and 12. We hypothesized an increase in the $\Delta I_{p,a}$ with increasing number of PAH/DNA bilayers because more aptamer present in the film would lead to an increase to the amount of quinine binding. Figure 3.6 shows the $\Delta I_{p,a}$ of the three compositions of the film. Results show that there is a slight increase in the $\Delta I_{p,a}$ as the number of PAH/DNA-aptamer bilayers increases. This effect

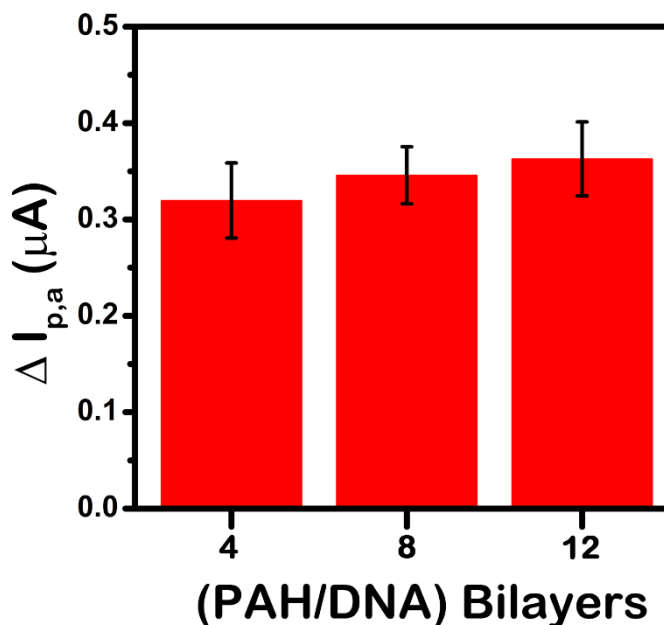


Figure 3.6. Response of platform in varying bilayers of PAH/DNA. A slight increase in ΔI_{pa} is observed when the number of PAH/DNA bilayers is increased from 4 to 12. Experiments were done in triplicate with SEM as error bars.

however is not significant and the small difference in $\Delta I_{p,a}$ suggests that the number of PAH/DNA-aptamer bilayers can be varied without sacrificing functionality.

More PAH/DNA-aptamer bilayers do not yield an increase in permeability. This effect could be due to the movement of $\text{Fe}(\text{CN})_6^{3-}/\text{Fe}(\text{CN})_6^{4-}$ through the film. A proposed mechanism consists of the “hopping” of ions from between positively charged sites to reach the electrodes.^[86b] As more film is added, more positively charged sites are available however the thickness of the film is increasing too. The increasing film thickness may counteract the effect of increasing positive charges.

3.3.5 Ionic Interference

The ability of a sensor to work in the presence of species other than the target makes it highly desirable for field analysis where sample preparation is minimal. We carried out ion

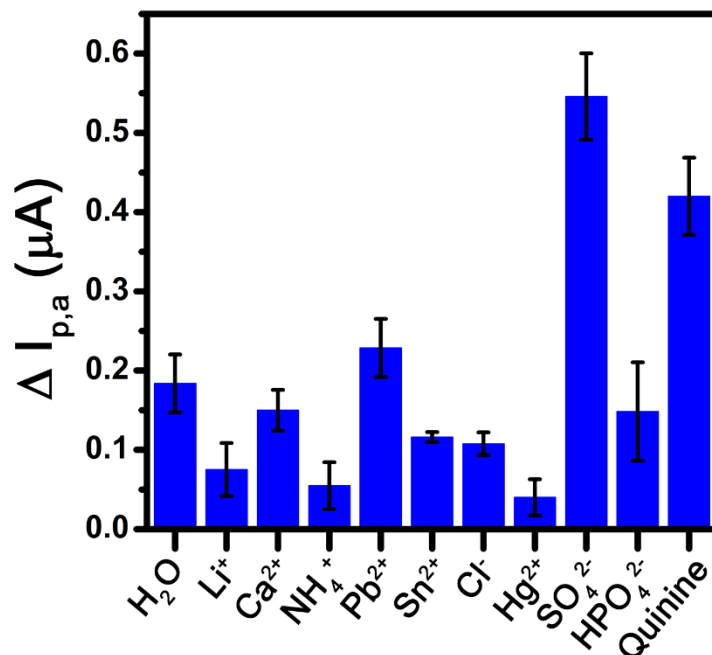


Figure 3.7. Interference experiments characterized with cyclic voltammetry. (a) $\Delta I_{p,a}$ is obtained for the films exposed to a range of anions and cations with concentration of 1 mM. Sulfate is the only species which gives false positive results. The rest of the ions have responses comparable to the control (H_2O). Error bars are SEM.

interference experiments to investigate the stability of the sensing platform, as in the colorimetric experiments. A series of platforms incubated with the various ions have their responses, $\Delta I_{p,a}$, measured and compared with control and quinine. Results presented in figure 3.7 show that the $\Delta I_{p,a}$ of most ions is similar to or lower than the control. Sulfate ions however give a false positive response of $0.55 \pm 0.04 \mu\text{A}$. Both methods of characterization, UV-visible and cyclic voltammetry, are in agreement and show that sulfate ions interfere with the platform. Conversely, mercury (II) ions do not show interference when the films are characterised with cyclic voltammetry. The absence of the effects of mercury (II) is due to the absence of the nanoparticles.

To improve the response of the platform incubated with sulfate ions, we precipitated the sulfate ions using BaCl_2 prior to immersion. Figure 3.8 compares the responses of the platform

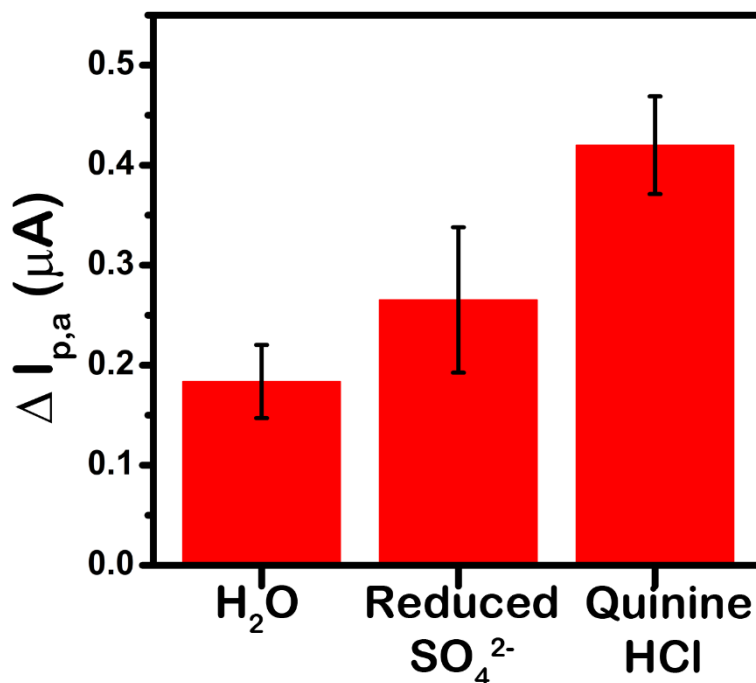


Figure 3.8. Sulfate ions are precipitated with BaCl_2 prior to incubation with the platform. A smaller response is observed from the platform when sulfate ions are removed from solution. Experiments done in triplicate with SEM as error bars.

exposed to water, solution with sulfate was precipitated, and quinine. Precipitation of sulfate ions leads to a decrease of $\Delta I_{p,a}$ from $0.55 \pm 0.04 \mu\text{A}$ (Figure 3.7) to $0.26 \pm 0.07 \mu\text{A}$ (Figure 3.8). The response is now comparable to the control, $0.19 \pm 0.03 \mu\text{A}$. Hence interferences from ions can be remediated by pre-treatment of the solution.

3.3.6 Effect of Aptamer Folding

One of our hypotheses is that the structural change during target binding in the MN19 aptamer enhances the rearrangement of the charges on the film. The roles MN19 and MN4 aptamers were compared again using cyclic voltammetry. Both aptamers have a three-stem structure and the quinine binds in the pocket where the three-way junction forms (Scheme 2.2). Similar to the colorimetric method, the response of the aptamers was measured and compared. This test determines if the structural change in the MN19 aptamer is crucial for a response.

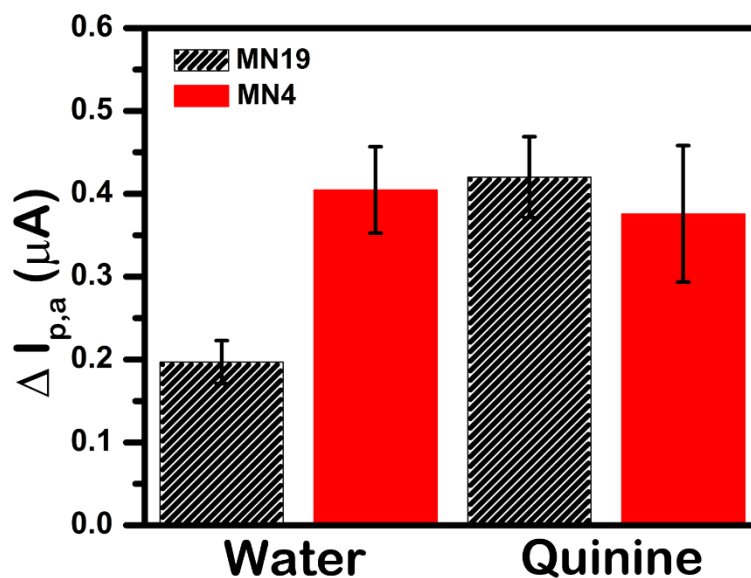
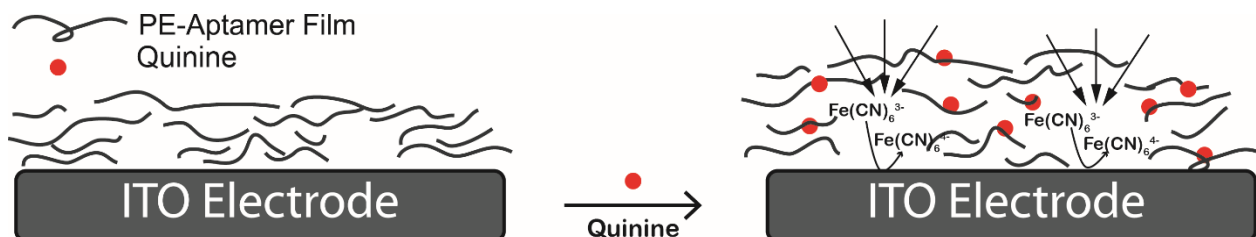


Figure 3.9. $\Delta I_{p,a}$ of films comprising with the two versions of the same aptamer. MN19 aptamer folds into a three stem junction when binding to quinine and MN4 aptamer has a pre formed three stem junction and does not change when binding. An increase in $\Delta I_{p,a}$ is observed when the structure changing aptamer MN19 is used. Experiments done in triplicate for MN4 and SEM is used for error bars.

We performed experiments where the MN19 aptamer is substituted with the MN4. From the initial scans, the anodic peak currents from the modified electrodes were in the 0.2 - 0.5 μA range. These initial peak currents suggest that, after deposition, films constructed with both the MN19 and MN4 have very similar structures. The scans after quinine binding tell a different story. Contrary to the films with MN19 aptamer, the responses for the MN4 film exposed to water vs quinine are similar (Figure 3.9). The MN4 film incubated in water has a $\Delta I_{p,a}$ of $0.40 \pm 0.05 \mu\text{A}$ and the MN4 film incubated in 350 μM Quinine has a $\Delta I_{p,a}$ of $0.37 \pm 0.08 \mu\text{A}$. Unlike when the MN19 aptamer is used, an electrochemical response was not obtained with the MN4 aptamer.

The increase in peak current after incubation with quinine may lie with the way the films are deposited initially. With the deposition of the first few layers the film is very porous and the effective coverage of the first two layers is very small. Areas of the electrodes, where deposition did not occur, are present. These areas get smaller and further apart from each other with increasing number of bilayers. Eventually they become pinholes which are covered with the final layers of the film.^[90] Scheme 3.1 illustrates these pinholes in the film. After incubation, the pinholes are more exposed. The difference in response between the platforms with different aptamers is that during target binding the structural change is absent from the MN4 aptamer. With the MN4 aptamer, quinine could bind however, the swelling of the films proceeds normally leading to a similar response from the film in quinine and in water. With the MN19 aptamer, the folding may



Scheme 3.1 Film assembly on ITO electrode. Uneven film deposition leads to exposed areas of electrodes. Target binding causes swelling of the film and increases the diffusion of ferricyanide to the electrode surface. The increase in diffusion is observed as an increase in peak current in cyclic voltammograms.

lead to the rearrangement of the charges in the film which in turn lead to greater permeability. This experiment reinforces the idea that for a functional platform, an aptamer that undergoes a structural change upon binding is crucial.

3.3.7 Peak Potentials and Diffusion Coefficients

In addition to testing out sensing performance, CV was used to examine the nature of the redox process. It can provide information on the reversibility of electron transfer and also on film deposition. The redox potentials of ferri-ferrocyanide on bare ITO electrodes were determined to be 0.223 ± 0.001 V and 0.124 ± 0.001 V against Ag/AgCl reference for anodic and cathodic peaks respectively, in line with reported values (0.24 V and 0.12 V).^[82] However with polyelectrolyte-aptamer covered electrodes, the redox potentials shift to more positive values at 0.345 ± 0.002 V and 0.248 ± 0.001 V. The difference between reduction and oxidation peak potentials also increases from 99 mV for bare electrode to 120 mV when PE-aptamer films were deposited. These observations are consistent with literature.^[86b] Smaller peak separation means better reversibility, due better access of the redox active species to the electrode. Film deposition reduces the effective area of the electrode leading to an increase in peak separation.^[86a] We also observed an increase in peak potentials after the electrodes were incubated in solutions: before incubation, the potentials are 0.345 ± 0.002 V for the anodic peak and 0.248 ± 0.001 V for the cathodic peak; after incubation, the peak potentials shift to 0.404 ± 0.002 V for the anodic peak and 0.274 ± 0.004 V for the cathodic peak. The peak shift shows that the film on the surface of the electrodes is changing during incubation, influencing the transport of ferricyanide.

Diffusion coefficients of the $\text{Fe}(\text{CN})_6^{4-}$ were extrapolated from the anodic peak currents using equation 3.1. After the deposition of the polyelectrolyte-aptamer film, the diffusion coefficient of ferrocyanide was $2.78 \times 10^{-7} \text{ cm}^2/\text{s}$. Once the target was introduced to the film, the anodic peak current increased and the diffusion coefficient was $1.36 \times 10^{-6} \text{ cm}^2/\text{s}$. According to equation 3.1, the current is proportional to $D^{1/2}$. Therefore, the diffusion of the $\text{Fe}(\text{CN})_6^{4-}$ in the quinine bound film, is 4.9 fold greater than the control film. These results show that the binding of the target to the film increases its permeability.

To investigate the reversibility of the redox process, we obtained cyclic voltammograms of electrodes modified with polyelectrolyte-aptamer film at different scan rates. The scan rate varied from 0.01 V/s to 1 V/s. Figure 3.10a shows the voltammograms as the scan rate increases. The inset in figure 3.11a shows the anodic and cathodic peak currents as a function of the square root of the scan rate. A linear response is observed and it shows that oxidation and reduction at the

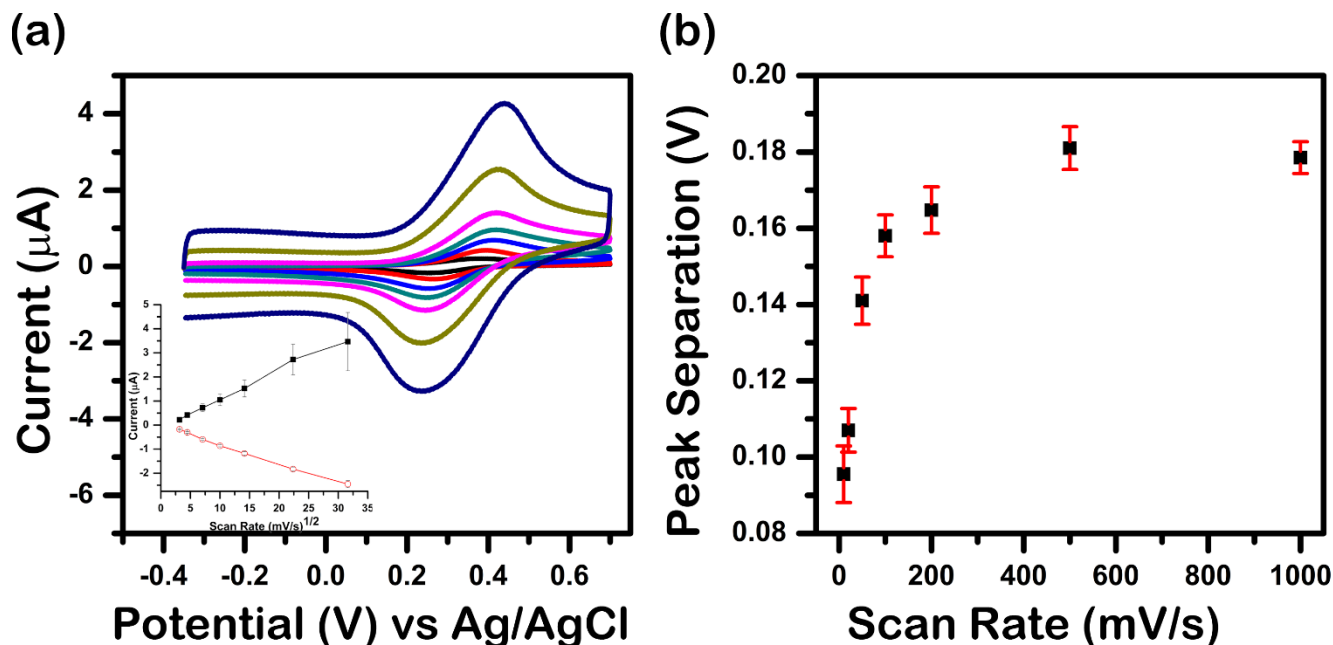


Figure 3.10. Scan rate dependence experiment of an ITO electrode modified with polyelectrolyte-aptamer film. (a) Cyclic voltammograms at increasing scan rates (10mV/s to 1000mV/s) of an electrode modified with polyelectrolyte-aptamer film. Inset shows linear dependence of peak currents with square root of scan rate. (b) Effect of scan rate on peak separation. Results show triplicate experiments with SEM as error bars.

electrode are diffusion controlled processes. The peak separation however increases with increasing scan rate (Figure 3.10b). At slow scan rates, 0.01 V/s, the peak separation is 96 ± 7 mV. The separation increases to 179 ± 4 mV with a scan rate of 1 V/s. These results suggest a reversible electron transfer mechanism at slow scan rates, and a quasi-reversible or irreversible mechanism at fast scan rates. Another observation that suggests a quasi-reversible system is the cathodic/anodic peak current ratio. The cathodic peak current is $76 \pm 2\%$ of the anodic peak current at scan rate of 0.1 V/s.

3.4 Conclusions

Cyclic voltammetry experiments confirm the deposition of the film on the electrode. The magnitude of the peak currents decreases with increasing number of bilayers. Optimization experiments show that four base bilayers of PAH/PSS are required for a reproducible response to be generated. The variation of the PAH/DNA-aptamer bilayers does not significantly change the response of the platform. More importantly, the results from the electrochemical study corroborate the findings from the colorimetric study. In addition we provide insight on the type of aptamer that can be used for this platform. By exploiting the difference in secondary structure formation between the aptamers, we show that the aptamer must undergo conformational changes to obtain a response from the film.

CHAPTER 4: Outlook and Future Work

4.1 Summary

This work has provided detailed insight on polyelectrolyte-aptamer films as potential recognition elements for biosensors. The underlying working principle of these films is the control of their permeability achieved via the incorporation of a DNA aptamer. The binding of the target to aptamer that changes its structure leads to more permeable films. For biosensing applications, these films can be easily integrated with a transducer without chemical functionalization to produce a signal. The target of interest of the films can be easily transformed by replacing the aptamer, as we demonstrated by replacing the original sulforhodamine B aptamer with the cocaine/quinine binding aptamer. When the film was integrated with gold-coated plasmonic nanoparticles, the binding of quinine increases the film's permeability leading to faster diffusion of oxidizing molecules to the nanoparticles. These molecules change the size and shape of nanoparticles to produce a colorimetric signal.

The optical detection method was improved by replacing the etchant couple, iodide/triiodide, with ferricyanide. The detection range of the target (quinine) is 50 μM to 250 μM . Interference experiments showed the platform retains its integrity in the presence of various monovalent and divalent ions, with the exception sulfate and mercury (II). Further investigation concluded that mercury (II) ions interact with nanoparticles while sulfate ions interact with the polyelectrolyte aptamer films. The platform was analyzed using two aptamers, MN19 and MN4, which differ only in structure changing ability upon interaction with the target. The results showed that the increase in permeability of the film is a direct consequence of the conformational changes in the aptamer.

We show the ability of the polyelectrolyte-aptamer film to be integrated in electrochemical systems by monitoring its permeability via cyclic voltammetry. The films were deposited on ITO electrodes and the electrochemical signal consisted of the difference in peak currents before and after target binding. A similar effective concentration range was obtained, 0 - 250 μM of quinine, which is in agreement with the optical method. Sulfate ions were determined to be an interfering species producing false positive responses. We showed that the interference of sulfate can be reduced by precipitating prior to measurement. In the absence of the nanoparticles mercury ions did not interfere with the platform. Experiments that test for non-specific binding show that the quinine binds to the MN19 aptamer without interacting with the electrode and the polyelectrolyte film. Results are in good agreement between the two methods and suggest that an aptamer that changes structure upon binding is required for a functional platform. The close agreement between the optical and electrochemical method shows that polyelectrolyte-aptamer films have great potential for sensing applications.

4.2 Outlook and Future Work

This work provides a basis for future applications of polyelectrolyte-aptamer films. The target of the films can be tailored by exchanging the aptamers. However, not all aptamers can affect the permeability of the film; only the ones that change structure. Future work involves further adaptation of the platform for a different analyte and development of a system where this setup can be utilized outside of the lab. With a few simple modifications, this platform provides a wide range of possibilities for sensing.

The control in permeability of the films on printed electrodes is a powerful tool which can be used for field testing. Additionally, polyelectrolyte films with different aptamers can be

assembled on electrode arrays to provide analysis of multiple species in a complex sample. These films can be directly assembled on the electrodes or they can be transfer printed with polydimethylsiloxane (PDMS). The assembly of the films on transparent ITO provides additional features to the biosensing method as optical signals such as fluorescence and absorbance can be concomitantly observed in addition to the electrochemical signal.

The polyelectrolyte-aptamer films may also be valuable in therapeutic applications. The control of permeability of these films can be exploited in microcapsules for drug delivery. When targeted to bind to cancer biomarkers, the capsules can be used for drug delivery in which the drug release occurs in the presence of biomarkers only, thus increasing the efficacy of the drug. Further development of polyelectrolyte aptamer films would be invaluable for medical fields in addition to providing new opportunities for the development of portable optical and electrochemical sensing devices.

References

- [1] A. J. Bandodkar, J. Wang, *Trends Biotechnol.* **2014**, *32*, 363-371.
- [2] G. Decher, *Science* **1997**, *277*, 1232-1237.
- [3] Y. Sultan, M. C. DeRosa, *Small* **2011**, *7*, 1219-1226.
- [4] K. E. Fong, L.-Y. L. Yung, *Nanoscale* **2013**, *5*, 12043-12071.
- [5] R. Stoltenburg, C. Reinemann, B. Strehlitz, *Biom Eng* **2007**, *24*, 381-403.
- [6] G. Decher, J.-D. Hong, *Makromol Symp* **1991**, *46*, 321-327.
- [7] G. Decher, M. Eckle, J. Schmitt, B. Struth, *Curr Opin Colloid Int* **1998**, *3*, 32-39.
- [8] D. A. Mortimer, *Polym. Int.* **1991**, *25*, 29-41.
- [9] W.-C. Liao, C.-H. Lu, R. Hartmann, F. Wang, Y. S. Sohn, W. J. Parak, I. Willner, *ACS Nano* **2015**.
- [10] M. Schönhoff, V. Ball, A. R. Bausch, C. Dejugnat, N. Delorme, K. Glinel, R. v. Klitzing, R. Steitz, *Colloid Surface A* **2007**, *303*, 14-29.
- [11] A. Plech, T. Salditt, C. Münster, J. Peisl, *J Colloid Interf Sci* **2000**, *223*, 74-82.
- [12] S. T. Dubas, J. B. Schlenoff, *Macromolecules* **1999**, *32*, 8153-8160.
- [13] D. T. Haynie, L. Zhang, W. Zhao, J. S. Rudra, *Nanomed-Nanotechnol* **2006**, *2*, 150-157.
- [14] A. V. Dobrynin, M. Rubinstein, *Prog Polym Sci* **2005**, *30*, 1049-1118.
- [15] Y. Zhang, P. S. Cremer, *Curr Opin Chem Biol* **2006**, *10*, 658-663.
- [16] R. R. Costa, J. F. Mano, *Chem Soc Rev* **2014**, *43*, 3453-3479.
- [17] T. Boudou, T. Crouzier, K. Ren, G. Blin, C. Picart, *Adv. Mater.* **2010**, *22*, 441-467.
- [18] F. Caruso, D. N. Furlong, K. Ariga, I. Ichinose, T. Kunitake, *Langmuir* **1998**, *14*, 4559-4565.
- [19] D. M. Sullivan, M. L. Bruening, *J Membrane Sci* **2005**, *248*, 161-170.

- [20] F. Caruso, *Adv. Mater.* **2001**, *13*, 11-22.
- [21] M. Tarabia, H. Hong, D. Davidov, S. Kirstein, R. Steitz, R. Neumann, Y. Avny, *J Appl Phys* **1998**, *83*, 725-732.
- [22] L. Chen, X. Zeng, A. R. Ferhan, Y. Chi, D.-H. Kim, G. Chen, *Chem Commun* **2015**, *51*, 1035-1038.
- [23] P. M. Biesheuvel, T. Mauser, G. B. Sukhorukov, H. Möhwald, *Macromolecules* **2006**, *39*, 8480-8486.
- [24] O. I. Vinogradova, O. V. Lebedeva, K. Vasilev, H. Gong, J. Garcia-Turiel, B.-S. Kim, *Biomacromolecules* **2005**, *6*, 1495-1502.
- [25] R. M. Iost, F. N. Crespilho, *Biosens Bioelectron* **2012**, *31*, 1-10.
- [26] D. H. J. Bunka, P. G. Stockley, *Nat Rev Microbiol* **2006**, *4*, 588-596.
- [27] T. Hermann, D. J. Patel, *Science* **2000**, *287*, 820-825.
- [28] W. G. Purschke, F. Radtke, F. Kleinjung, S. Klussmann, *Nucleic Acids Res* **2003**, *31*, 3027-3032.
- [29] D. Proske, S. Gilch, F. Wopfner, H. M. Schätzl, E.-L. Winnacker, M. Famulok, *ChemBioChem* **2002**, *3*, 717-725.
- [30] S. M. Nimjee, C. P. Rusconi, B. A. Sullenger, *Annu Rev Med* **2005**, *56*, 555-583.
- [31] D. M. Held, J. D. Kissel, J. T. Patterson, D. G. Nickens, D. H. Burke, *Front Biosci* **2006**, *11*, 89-112.
- [32] aW. Zhao, W. Chiuman, M. A. Brook, Y. Li, *ChemBioChem* **2007**, *8*, 727-731; bJ. Liu, Y. Lu, *Angew. Chem. Int. Ed.* **2006**, *45*, 90-94.
- [33] B. R. Baker, R. Y. Lai, M. S. Wood, E. H. Doctor, A. J. Heeger, K. W. Plaxco, *J Am Chem Soc.* **2006**, *128*, 3138-3139.

- [34] S. Samanta, S. Martha, K. Parida, *ChemCatChem* **2014**, *6*, 1453-1462.
- [35] B. Malile, J. I. L. Chen, *J Am Chem Soc* **2013**, *135*, 16042-16045.
- [36] B. Srinivasan, S. Tung, *J Lab Autom* **2015**, *20*, 365-389.
- [37] F. Long, A. Zhu, H. Shi, *Sensors* **2013**, *13*, 13928.
- [38] B. V. Chikkaveeraiah, A. Bhirde, N. Y. Morgan, H. S. Eden, X. Chen, *ACS nano* **2012**, *6*, 6546-6561.
- [39] J. Katrlík, A. Pizzariello, V. r. Mastihuba, J. Švorc, M. Stred'anský, S. Miertuš, *Anal Chim Acta* **1999**, *379*, 193-200.
- [40] J. Wang, J. R. Fernandes, L. T. Kubota, *Anal. Chem.* **1998**, *70*, 3699-3702.
- [41] K. Bizet, C. Gabrielli, H. Perrot, *Analisis* **1999**, *27*, 609-616.
- [42] J.-M. Kauffmann, G. G. Guilbault, *Bioprocess Tech* **1990**, *15*, 63-82.
- [43] W. Zhao, J.-J. Xu, H.-Y. Chen, *Electroanal* **2006**, *18*, 1737-1748.
- [44] J. Wang, *J Pharm Biomed Anal* **1999**, *19*, 47-53.
- [45] L. Wide, *Upsala J Med Sci* **2005**, *110*, 193-216.
- [46] D. Mark, S. Haeberle, G. Roth, F. von Stetten, R. Zengerle, *Chem Soc Rev* **2010**, *39*, 1153-1182.
- [47] C. D. Chin, V. Linder, S. K. Sia, *Lab Chip* **2012**, *12*, 2118-2134.
- [48] P. Leman, D. Guthrie, R. Simpson, F. Little, *Emerg Med J* **2004**, *21*, 452-456.
- [49] N. Nath, A. Chilkoti, *Anal. Chem.* **2002**, *74*, 504-509.
- [50] T. C. Chu, F. Shieh, L. A. Lavery, M. Levy, R. Richards-Kortum, B. A. Korgel, A. D. Ellington, *Biosens. Bioelectron.* **2006**, *21*, 1859-1866.
- [51] K. M. Mayer, J. H. Hafner, *Chem Rev* **2011**, *111*, 3828-3857.
- [52] Z. Xuming, C. Yu Lim, L. Ru-Shi, T. Din Ping, *Rep Prog Phys* **2013**, *76*, 046401.

- [53] E. Petryayeva, U. J. Krull, *Anal Chim Acta* **2011**, 706, 8-24.
- [54] aG. Liu, Y. Hou, X. Xiao, G. Zhang, *J Phys Chem B* **2010**, 114, 9987-9993; K. A. Willets, R. P. Van Duyne, *Annu Rev Physl Chem* **2007**, 58, 267-297.
- [55] A. J. Haes, S. Zou, G. C. Schatz, R. P. Van Duyne, *J Phys Chem B* **2004**, 108, 6961-6968.
- [56] E. Hutter, J. H. Fendler, *Adv Mater* **2004**, 16, 1685-1706.
- [57] M. Maillard, P. R. Huang, L. Brus, *Nano Lett* **2003**, 3, 1611-1615.
- [58] C. Gao , Z. Lu , Y. Liu , Q. Zhang, M. Chi, Q. Cheng, Y. Yin, *Angew Chem Int Ed* **2012**, 51, 5629-5633.
- [59] L. Chen, X. Fu, W. Lu, L. Chen, *ACS App Mat Int* **2012**, 5, 284-290.
- [60] X. Wang, L. Chen, L. Chen, *Microchim Acta* **2014**, 181, 105-110.
- [61] C. B. Gao, Z. D. Lu, Y. Liu, Q. Zhang, M. F. Chi, Q. Cheng, Y. D. Yin, *Angew Chem Int Ed* **2012**, 51, 5629-5633.
- [62] J. Zeng, X. H. Xia, M. Rycenga, P. Henneghan, Q. G. Li, Y. N. Xia, *Angew Chem Int Ed* **2011**, 50, 244-249.
- [63] Y. Sultan, R. Walsh, C. Monreal, M. C. DeRosa, *Biomacromolecules* **2009**, 10, 1149-1154.
- [64] C. M. Copley, M. Rycenga, F. Zhou, Z.-Y. Li, Y. Xia, *J Phys Chem C* **2009**, 113, 16975-16982.
- [65] Y. Xia, X.-M. Zhao, E. Kim, G. M. Whitesides, *Chem Mater* **1995**, 7, 2332-2337.
- [66] J. Zhai, Y. Zhai, S. Dong, *Colloid Surface A* **2009**, 335, 207-210.
- [67] S. L. Clark, M. F. Montague, P. T. Hammond, *Macromolecules* **1997**, 30, 7237-7244.

- [68] Y. Liu, M. Zhao, D. E. Bergbreiter, R. M. Crooks, *J Am Chem Soc* **1997**, *119*, 8720-8721.
- [69] G. Wang, Q. Zhao, X. Kang, X. Guan, *J Phys Chem B* **2013**, *117*, 4763-4769.
- [70] J. R. N. McLean, D. H. Blakey, G. R. Douglas, J. G. Kaplan, *Mutat Res Lett* **1983**, *119*, 195-201.
- [71] A. Hartwig, *Environ Health Perspect* **1994**, *102*, 45-50.
- [72] J. T. T. Pang, I. M. Ritchie, *Electrochim Acta* **1982**, *27*, 683-689.
- [73] K. V. Katok, R. L. D. Whitby, T. Fukuda, T. Maekawa, I. Bezverkhyy, S. V. Mikhalovsky, A. B. Cundy, *Angew Chem Int Ed* **2012**, *51*, 2632-2635.
- [74] J. J. Harris, J. L. Stair, M. L. Bruening, *Chem Mater* **2000**, *12*, 1941-1946.
- [75] M. N. Stojanovic, P. de Prada, D. W. Landry, *J Am Chem Soc* **2001**, *123*, 4928-4931.
- [76] O. Reinstein, M. Yoo, C. Han, T. Palmo, S. A. Beckham, M. C. J. Wilce, P. E. Johnson, *Biochemistry* **2013**, *52*, 8652-8662.
- [77] J. Wang, *Acc Chem Res* **2002**, *35*, 811-816.
- [78] a) J. Wang, *TrAC, Trends Anal Chem* **2002**, *21*, 226-232; b) J. Wang, *Analytical electrochemistry*, John Wiley & Sons, **2006**.
- [79] P. Kissinger, W. R. Heineman, *Laboratory Techniques in Electroanalytical Chemistry, revised and expanded*, CRC press, **1996**.
- [80] T. H. Silva, V. Garcia-Morales, C. Moura, J. A. Manzanares, F. Silva, *Langmuir* **2005**, *21*, 7461-7467.
- [81] H. Hillebrandt, G. Wiegand, M. Tanaka, E. Sackmann, *Langmuir* **1999**, *15*, 8451-8459.
- [82] C. Thiruppathiraja, V. Saroja, S. Kamatchiammal, P. Adaikkappan, M. Alagar, *J Environ Monitor* **2011**, *13*, 2782-2787.

- [83] A. J. Bard, L. R. Faulkner, *Electrochemical methods: fundamentals and applications, Vol. 2*, Wiley New York, **1980**.
- [84] P. T. Kissinger, W. R. Heineman, *J Chem Educ* **1983**, *60*, 702.
- [85] F. N. Crespilho, V. Zucolotto, O. N. Oliveira Jr, F. C. Nart, *Int J Electrochem Sci* **2006**, *1*, 194.
- [86] a) J. J. Harris, M. L. Bruening, *Langmuir* **1999**, *16*, 2006-2013; b) H. Lindholm-Sethson, S., *Electrochim. Acta* **1999**, *45*, 845-853.
- [87] M. A. D. Neves, O. Reinstein, M. Saad, P. E. Johnson, *Biophys Chem* **2010**, *153*, 9-16.
- [88] S. Slavkovic, M. Altunisik, O. Reinstein, P. E. Johnson, *Biorg Med Chem* **2015**, *23*, 2593-2597.
- [89] A. E. El Haitami, D. Martel, V. Ball, H. C. Nguyen, E. Gonthier, P. Labbé, J.-C. Voegel, P. Schaaf, B. Senger, F. Boulmedais, *Langmuir* **2009**, *25*, 2282-2289.
- [90] S. V. P. Barreira, V. García-Morales, C. M. Pereira, J. A. Manzanares, F. Silva, *J Phys Chem B* **2004**, *108*, 17973-17982.